

**Development of a Novel Quantitative Method for Protein
S-Palmitoylation and Exploration of Depalmitoylating
Enzymes for PSD-95**

Atsushi Sekiya

Doctor of Philosophy

Department of Physiological Sciences

School of Life Science

The Graduate University for Advanced Studies (SOKENDAI)

2015

Acknowledgements

I am deeply grateful to my supervisors, Drs. Masaki Fukata and Yuko Fukata [Division of Membrane Physiology, National Institute for Physiological Sciences (NIPS) and SOKENDAI], for all their support and advice for my study. I am grateful to Mr. Tatsuro Murakami (Division of Membrane Physiology, NIPS and SOKENDAI) for collaborating with me to explore the depalmitoylating enzymes. I would like to thank the members of Fukata laboratory, Dr. Norihiko Yokoi, Dr. Shinichiro Oku, Dr. Toshika Ohkawa, Mr. Naoki Takahashi, Ms. Yumi Suzuki, and Ms. Mie Watanabe for kind supports.

I would like to express appreciations to my dissertation committee members, Drs. Motohiro Nishida (Division of Cardiocirculatory Signaling, NIPS and SOKENDAI), Yoshihiro Kubo (Division of Biophysics and Neurobiology, NIPS and SOKENDAI), and Mitsuharu Hattori (Graduate School of Pharmaceutical Sciences, Nagoya City University).

I would like to thank Dr. Kenta Kobayashi and Ms. Rie Kageyama (Section of Viral Vector Development, NIPS) for generating adeno-associated virus vectors.

I would like to thank Dr. Takaki Koide (Graduate School of Advanced Science and Engineering, Waseda University) for giving me a lot of valuable advice when I was a graduate student of the master's course.

This research was supported by Japan Society for the Promotion of Science (JSPS)

Grant-in-Aid for JSPS Fellows DC1 Number 24-2352.

Lastly, I would like to thank my family for always supporting me.

Contents

Summary	4
Abbreviations	8
Introduction	11
Materials and Methods	16
Results	
<u>Chapter 1</u>	
Development of a novel quantitative method for <i>S</i> -palmitoylation	34
<u>Chapter 2</u>	
Exploration of novel depalmitoylating enzymes for PSD-95	45
Discussion	55
Figures and Figure legends	63
Tables	87
References	94

Summary

Protein *S*-palmitoylation is one of the reversibly regulated post-translational modifications. *S*-palmitoylation is an addition of a lipid palmitate to a specific cysteine residue via a thioester bond and plays a critical role in protein trafficking and function. *S*-palmitoylation modifies various types of proteins such as signaling molecules, ion channels, and scaffolding proteins. Post-synaptic scaffolding protein PSD-95 is one of the most intensively studied *S*-palmitoylated proteins and *S*-palmitoylation of PSD-95 is essential for its post-synaptic targeting. The palmitate cycling on palmitoyl proteins is dynamically regulated by palmitoyl acyltransferases (PATs) and palmitoyl-protein thioesterases (PPTs). Although the DHHC protein family has recently emerged as genetically conserved PATs, PPTs (*i.e.*, depalmitoylating enzymes) remain controversial since 1970s. Thus, the regulatory mechanism of reversible *S*-palmitoylation is incompletely understood. Another important issue in the *S*-palmitoylation research is the lack of the quantitative method to address *S*-palmitoylation stoichiometries of proteins in cells or tissues. Here, I challenged these two fundamental questions. In **Chapter 1**, I developed a novel method, acyl-PEGyl exchange gel shift (APEGS) assay, which allows quantification of the number of *S*-palmitoylation sites in palmitoylated proteins and their *in vivo* palmitoylation stoichiometries. In **Chapter 2**, I explored PSD-95 palmitoyl-protein thioesterases (P-PPTs).

The principle of the APEGS assay I developed is that the exchange of palmitates with

high-molecular weight polymers, polyethylene glycols (PEGs), at the reversibly palmitoylated thiols induces the mobility shift of *S*-palmitoylated proteins on sodium dodecyl sulfate-polyacrylamide gel electrophoresis. The APEGS assay is composed of four chemical reactions: 1) reduction of intra- and intermolecular disulfide bonds by tris-(2-carboxyethyl) phosphine; 2) blockade of non-palmitoylated cysteine residues with a thiol specific modification reagent, *N*-ethyl maleimide; 3) cleavage of palmitoyl-cysteine thioester bonds with hydroxylamine treatment; and 4) introduction of maleimide-conjugated PEGs into newly exposed cysteines. I first optimized the conditions of individual chemical reactions and demonstrated that the extent of mobility shift observed in the APEGS assay depends on the number of *S*-palmitoylation sites using PSD-95 as a model substrate. Then, I applied this APEGS assay to various *S*-palmitoylated proteins in cultured rat hippocampal neurons and quantified the number of sites and stoichiometries of *S*-palmitoylation of previously reported palmitoyl proteins, including PSD-95, Hras, and G α_q . I for the first time found that about 80% of PSD-95 was di-palmitoylated in neurons and that the rest (~20%) of PSD-95 was not palmitoylated in neurons. I also found that depalmitoylation of PSD-95 was faster than that of Hras in neurons and that two palmitates on PSD-95 were cleaved almost at the same time with a half-life of 1.8 ± 0.4 hours. Furthermore, the mathematical simulation suggests that the palmitoylation reaction of PSD-95 is four times as fast as the depalmitoylation reaction.

Next, I explored PSD-95 depalmitoylating enzymes, P-PPTs. Because thioesterases mainly

belong to huge serine hydrolase superfamily including proteases, esterases, and lipases, I attempted to examine whether members of uncharacterized serine hydrolases have PPT activities. I isolated 38 genes of mouse or rat serine hydrolases and examined their effects on the palmitoylation level of PSD-95 by a metabolic labeling assay with [³H]-palmitate in HEK293T cells. I found that 10 candidates showed activities to reduce PSD-95 palmitoylation levels. Importantly, these candidates belong to a distinct phylogenetic subgroup. I confirmed that these candidates were expressed in cultured rat hippocampal neurons and then investigated their subcellular localization. I found that only three members were uniquely localized at/near the post-synaptic membranes in rat hippocampal neurons, which were referred to as post-synaptic P-PPTs in this study. Since PSD-95 is expected to be depalmitoylated mainly at post-synaptic membranes, I selected post-synaptic P-PPTs for further analysis. I predicted and experimentally verified the catalytic triad amino acid residues of post-synaptic P-PPTs. I found that an ectopically expressed post-synaptic P-PPT directly bound to PSD-95 and dramatically reduced the palmitoylation level of endogenous PSD-95 in neurons. Then, I prepared rat hippocampal neurons in which three post-synaptic P-PPTs or the other candidate proteins were knocked down by using microRNA encoding adeno-associated viruses and investigated their effects on the depalmitoylation process of PSD-95. However, the depalmitoylation process of PSD-95 was not largely changed under the present experimental condition. This result raises three possibilities: 1) insufficient knockdown, 2) molecular redundancy of P-PPTs, and 3) existence of other authentic

candidates.

In conclusion, I established a novel method APEGS that for the first time provides quantitative information about the number of sites and stoichiometry of *S*-palmitoylation *in vivo*. This method will widely and rapidly spread over the *S*-palmitoylation research. Furthermore, I obtained 10 candidate proteins for PSD-95 depalmitoylating enzymes and characterized post-synaptic P-PPTs. Thus, my study should contribute to elucidating the molecular mechanism for the reversible *S*-palmitoylation in diverse cellular processes.

Abbreviations

AadacI	arylacetamide deacetylase-like
AAV	adeno-associated virus
AAV-DJ	DJ-type AAV
ABE	acyl-biotinyl exchange
ABHD	α/β hydrolase domain containing
AMPA	α -amino-3-hydroxy-5-methyl-4-isoxazole propionic acid
APEGs	acyl-PEGyl exchange gel shift
APT	acyl-protein thioesterase
BCA	bichinchoninic acid
2-BP	2-bromopalmitate
BSA	bovine serum albumin
cDNA	complementary DNA
Cav1	caveolin1
CBB	coomassie brilliant blue
CM ppt	chloroform/methanol precipitation
5CS	palmitoylation-deficient ABHD17B, C10/11/14/15/18S
DHHC	Asp-His-His-Cys
DIV	days <i>in vitro</i>
DMEM	Dulbecco's modified Eagle medium
DNA	deoxyribonucleic acid
Dpp	dipeptidylpeptidase
EDTA	ethylenediamine tetraacetate
ER	endoplasmic reticulum

Faah	fatty acid amide hydrolase
Fasn	fatty acid synthase
FBS	fetal bovine serum
GFP	green fluorescent protein
GST	glutathione <i>S</i> -transferase
HA	hemagglutinin
HDFP	hexadecylfluorophosphonate
HEPES	4-(2-hydroxyethyl)-1-piperazine ethane sulfonic acid
hPF11	human Fc-fused PF11
HRP	horse radish peroxidase
IgG	immunoglobulin G
IP	immunoprecipitation
Lipe	hormone sensitive lipase
Lypla	lysophospholipase
Lyplal	Lypla-like
MAFP	methyl arachidonyl fluorophosphonate
MAGUK	membrane-associated guanylate kinase
miR/miRNA	microRNA
mRNA	messenger RNA
mPEG	maleimide conjugated PEG
NEM	<i>N</i> -ethyl maleimide
NIPS	National Institute for Physiological Sciences
<i>N</i> -myr	<i>N</i> -myristoylated ABHD17B, Src(1-20)/ABHD17B(21-288)
Pafah	platelet-activating factor acetylhydrolase

PAGE	polyacrylamide gel electrophoresis
Palm-B	palmostatin-B
PAT	palmitoyl acyltransferase
PBS	phosphate-buffered saline
PCR	polymerase chain reaction
PEG	polyethylene glycol
PGAP	post-glycosylphosphatidylinositol attachment to proteins
PMSF	phenyl methylsulfonyl fluoride
PNPLA	patatin-like domain containing
PPT	palmitoyl-protein thioesterase
P-PPT	PSD-95 PPT
PSD	post-synaptic density
PVDF	polyvinylidene difluoride
RNA	ribonucleic acid
RT	reverse transcription
SDS	sodium dodecyl sulfate
TARP	transmembrane AMPA receptor regulatory protein
TBS	tris-buffered saline
TCEP	tris-(2-carboxyethyl) phosphine
TE	thioesterase domain
Tex	testis expressed
TTBS	Tween20-containing TBS
vg	virus genome
WT	wild-type

Introduction

Reversibly regulated post-translational modifications of proteins such as protein phosphorylation play central roles in various cellular events. Lipid modifications that contain *S*-palmitoylation (El-Husseini and Brecht, 2002; Resh, 2006; Linder and Deschenes, 2007; Fukata and Fukata, 2010), *N*-myristoylation (Resh, 1999), and *S*-prenylation (Zhang and Casey, 1996) increase hydrophobicity of proteins to target them to various endomembranes and the plasma membrane. Among them, *S*-palmitoylation is another representative reversible modification of proteins. *S*-palmitoylation, also called *S*-acylation, is an addition of a fatty acid, mainly 16-carbon saturated palmitate, to a sulfhydryl group of a specific cysteine residue via a thioester linkage. *S*-palmitoylation was originally discovered in a study of viral glycoprotein-lipid interaction (Schmidt *et al.*, 1979). Since then, some representative substrates were reported such as heterotrimeric G protein α subunits ($G\alpha_s$, $G\alpha_q$, and $G\alpha_{i2}$) (Linder *et al.*, 1993; Parenti *et al.*, 1993), proto-oncogenic proteins H/Nras (Sefton *et al.*, 1982; Hancock *et al.*, 1989), and neuronal scaffolding protein PSD-95 (Topinka and Brecht, 1998). Recent global proteome studies have greatly expanded knowledge about the numbers and types of palmitoyl proteins, such as signaling molecules, enzymes, cytoskeletal proteins, ion channels and cell adhesion molecules, and so on (Kang *et al.*, 2008; Martin and Cravatt, 2009; Yang *et al.*, 2010; Martin *et al.*, 2011). Intriguingly, palmitoylated proteins significantly accumulate in specialized membrane structures of the cell, called membrane microdomains such as immunosynapses of immune cells, tight junctions of epithelial cells,

and pre/post-synapses in neurons. Increasing evidence proposes that *S*-palmitoylation is one of the most important factors of formation and maintenance of membrane microdomains (see reviews, Brown, 2006; Levental *et al.*, 2010).

Post-synapse, especially post-synaptic density (PSD), is a well-characterized membrane microdomain containing many types of proteins, glutamate receptors, synaptic adhesion molecules, and intracellular scaffolding proteins. PSD-95 is the most abundant and well-characterized *S*-palmitoylated scaffolding protein that has three PDZ domains and belongs to membrane-associated guanylate kinase (MAGUK) family (Cho *et al.*, 1992; Topinka and Bredt, 1998; Kim and Sheng, 2004). PSD-95 plays a central role in synaptic maturation and synaptic transmission through interactions with various PSD membrane proteins such as AMPA (α -amino-3-hydroxy-5-methyl-4-isoxazole propionic acid)-type glutamate receptor/TARP (transmembrane AMPA receptor regulatory protein) complex via its PDZ domains (Chen *et al.*, 2000). Overexpression of PSD-95 accelerates maturation of glutamatergic synapses of hippocampal neurons and selectively increases the AMPA receptor clustering and activity (El-Husseini *et al.*, 2000a). On the other hand, acute suppression of PSD-95 selectively decreases AMPA receptor clustering and activity (Elias *et al.*, 2006). Importantly, the dynamic and activity-dependent palmitate turnover occurs on PSD-95 at N-terminal two cysteines, Cys3 and Cys5, and regulates synaptic localization and function of PSD-95 (Topinka and Bredt, 1998; Craven *et al.*, 1999; El-Husseini *et al.*, 2002; Noritake *et*

al., 2009; Fukata *et al.*, 2013). In fact, irreversibly *N*-myristoylated PSD-95 chimera could not efficiently form post-synaptic clusters (Craven *et al.*, 1999; Fukata *et al.*, 2013), suggesting that the reversibility of *S*-palmitoylation is important to form the post-synaptic cluster of PSD-95.

It has been considered that reversible *S*-palmitoylation is catalyzed by two types of enzymes, palmitoyl acyltransferases (PATs; *i.e.*, palmitoylating enzymes) and palmitoyl-protein thioesterases (PPTs; *i.e.*, depalmitoylating enzymes). Asp-His-His-Cys (DHHC) motif-containing DHHC family members function as evolutionally conserved PATs. There are 24 DHHC proteins in mammal, many of which are shown to exhibit PAT activities (Fukata *et al.*, 2004; Fukata and Fukata, 2010). On the other hand, 4 enzymes, lysophospholipase 1 and 2 (Lypla1/2) that are also called acyl-protein thioesterase 1/2 (APT1/2; Duncan and Gilman, 1998; Tomatis *et al.*, 2010), Lypla-like 1 (Lyplal1; Tian *et al.*, 2012), and palmitoyl-protein thioesterase 1 (PPT1; Camp and Hofmann, 1993), were reported as putative PPTs using *in vitro* reconstitutions or overexpression systems. However, their physiological roles are still controversial and PPTs for PSD-95 have not yet been identified. Recently, Martin *et al.* reported that treatment with a synthetic serine hydrolase inhibitor hexadecylfluorophosphonate (HDFP) inhibits depalmitoylation of various proteins such as Nras, G α_q and MPPs (members of the MAGUK family), suggesting that HDFP-targets are potent candidates for unknown depalmitoylating thioesterases (Martin *et al.*, 2011). Thus, the

regulatory mechanism of reversible *S*-palmitoylation cycles is incompletely understood.

Lack of quantitative methods for *S*-palmitoylation is another unsolved problem. The information about the palmitoylation stoichiometries on endogenous proteins is very limited and also whether proteins are singly, doubly or multiply palmitoylated in cells has not yet been assessed. So far, two types of methods have been used for biochemical detection of *S*-palmitoylated proteins. First, metabolic labeling of proteins with [³H]-palmitate is the most classical and common assay (Schmidt *et al.*, 1979; Schlesinger *et al.*, 1980). Recently, non-radioactive metabolic labeling approaches have been developed, which take advantage of click chemistry with palmitate analogs, such as an ω -alkynyl palmitate (Charron *et al.*, 2009; Hannoush and Arenas-Ramirez, 2009; Martin and Cravatt, 2009; Martin *et al.*, 2011). These metabolic labeling methods require live cells and are unsuitable to determine the precise number of palmitoylated sites and the palmitoylation stoichiometry, because the level of label incorporation is usually very low. The second class of analytical methods is the chemical biotin-switch method called acyl-biotinyl exchange (ABE). Following a chemical exchange between palmitates on proteins and biotin moieties, biotinylated proteins are purified by avidin-conjugated beads and identified by western blotting or mass spectrometry (Driscoll and Green, 2004; Roth *et al.*, 2006; Wan *et al.*, 2007; Kang *et al.*, 2008; Yang *et al.*, 2010). This method allows sensitive detection of palmitoylated proteins in cells or tissues. However, since palmitoylated proteins are purified and detected regardless of their palmitoylated states

(mono-, di- or multiply palmitoylated), ABE could not provide quantitative information about the number of palmitoylation sites nor the palmitoylation stoichiometries. The quantitative method that overcomes previous limitations is awaited to investigate the dynamic process of reversible *S*-palmitoylation cycles, including characterization of PATs and identification of undefined PPTs.

In my doctoral thesis, I first developed a novel quantitative method for protein *S*-palmitoylation in **Chapter 1** to quantitatively understand the property of the palmitate cycling on PSD-95. I for the first time succeeded in quantifying the palmitoylation stoichiometry of PSD-95 in neurons and the dynamic depalmitoylation process of PSD-95. In **Chapter 2**, I explored PSD-95 PPTs (P-PPTs) and obtained promising candidates.

Materials and Methods

Contents

Materials	18
Antibodies	19
Plasmids	19
Cloning of serine hydrolase genes and plasmid construction	20
Mutagenesis	21
Cell culture and transfection	23
HEK293T cells	
Cultured rat hippocampal neurons	
Adeno-associated virus (AAV) vectors	24
Construction of microRNA vectors for AAV generation	
Generation of AAV vectors	
AAV infection into neurons	
Acyl-PEGyl exchange gel shift (APEGS) assay	26
SDS-PAGE and western blotting	27

Mathematical simulation	28
Steady-state palmitoylation cycle of PSD-95	
Step-wise depalmitoylation reaction of PSD-95	
Metabolic [³ H]-palmitate labeling assay	30
<i>In silico</i> structural predictions and sequence alignments	31
Immunofluorescence analysis and fluorescence microscopy	31
Immunoprecipitation (IP)	32
Real-time quantitative PCR	33

All animal studies described herein were reviewed and approved by the ethics committee at NIPS and were performed according to institutional guidelines concerning the care and handling of experimental animals.

Materials

The following maleimide conjugated polyethylene glycols (mPEGs) were used: mPEG with molecular weight ~1,000 g/mol, hereafter referred to as mPEG-1k (MM(PEG)₂₄, Thermo Fisher scientific, Waltham, MA); mPEG-2k (SUNBRIGHT ME-020MA, NOF, Tokyo, Japan); mPEG-5k (SUNBRIGHT ME-050MA, NOF); and mPEG-10k (methoxypolyethylene glycol maleimide ~10,000 g/mol, Sigma-Aldrich, St Louis, MO). *N*-ethyl maleimide (NEM), hydroxylamine hydrochloride, and tris-(2-carboxyethyl) phosphine (TCEP, Bond-breaker TCEP solution neutral pH) were purchased from Wako pure chemical (Tokyo, Japan), Sigma-Aldrich, and Thermo Fisher scientific, respectively. The following protease inhibitors were used: phenyl methylsulfonyl fluoride (PMSF, Nakarai tesque, Kyoto, Japan), leupeptin (Peptide Institute, Osaka, Japan), pepstatin A (Peptide Institute), and ethylenediamine tetraacetate (EDTA, Dojindo, Kumamoto, Japan). Palmitoylation inhibitor 2-bromopalmitate (2-BP) was purchased from Sigma-Aldrich. Lipase inhibitors, palmostatin-B (Palm-B), Orlistat, and methyl arachidonyl fluorophosphonate (MAFP) were purchased from Millipore (Billerica, MA), Wako pure chemical, and Sigma-Aldrich, respectively.

Antibodies

The following antibodies were used: rabbit polyclonal antibodies to green fluorescent proteins (GFP, Fukata laboratory, Tsutsumi *et al.*, 2009), PSD-95 (Fukata laboratory #9311, Noritake *et al.*, 2009), $G\alpha_{q/11}$ (Santa Cruz, Dallas, TX, sc-392), $G\alpha_s$ [Millipore (Chemicon), AB1639], caveolin1 (Cav1, Santa Cruz, sc-894), calnexin [Enzo Life Science (Stressgen), Farmingdale, NY, ADI-SPA-860]. Rabbit monoclonal antibody to Hras (Abcam, Cambridge, MA, Y132). Mouse monoclonal antibodies to hemagglutinin (HA, 12CA5, from Dr. Kozo Kaibuchi, Nagoya University), Flag (Sigma-Aldrich, M2), PSD-95 (Thermo Fisher scientific, 7E3-1B8), Nras (Santa cruz, F155), and SNAP25 [BioLegend (Sterberger), Dedham, MA, SMI81]. Rat monoclonal antibody to HA (Roche, Basel, Switzerland, 3F10). The recombinant antibody, human Fc-fused PF11 (hPF11) for palmitoylated PSD-95 was generated by Dr. Franck Perez (Institut Curie, Fukata *et al.*, 2013). The following secondary antibodies were used: horseradish peroxidase (HRP)-conjugated anti-rabbit IgG (GE healthcare, Little Chalfont, UK), HRP-conjugated anti-mouse IgG (GE healthcare), Cy3-conjugated anti-rat IgG (Jackson, West Grove, PA), DyLight 488-conjugated anti-human IgG Fc (Jackson), and Alexa Fluor 647-conjugated anti-mouse IgG (Life technologies, Carsbad, CA).

Plasmids

The following plasmids were used: pGW:rat PSD-95-GFP, pGW:rat PSD-95 C3/5S, and pEF-Bos:HA-GST for the metabolic labeling assay (Fukata *et al.*, 2004). pGW:rat

PSD-95-GFP was also used for generation of pCAGGS:PSD-95. pEGFP-C:mouse Hras (Fukata *et al.*, 2004) was used for generation of pCAGGS:Flag-Hras. pEF-Bos:HA-mouse DHHC3 (Fukata *et al.*, 2004) was used for validation of the APEGS assay.

Cloning of serine hydrolase genes and plasmid construction

To prepare mouse and rat brain total RNAs, mouse and rat whole brains were homogenized with Trizol reagent (Life technologies). The homogenate was mixed with chloroform for 2 min at room temperature. After centrifugation at 11,000 x g for 15 min at 4°C, upper phases were mixed with isopropanol for 10 min at room temperature. After centrifugation at 11,000 x g for 15 min at 4°C, supernatants were removed and pellets were rinsed with 75% ethanol. After centrifugation at 11,000 x g for 15 min at 4°C, supernatants were removed and pellets were dissolved in nuclease-free water. Complementary DNAs (cDNAs) were obtained by reverse transcription-polymerase chain reactions (RT-PCRs). Two microgram of total RNA was used for the first-strand cDNA synthesis with Superscript-III system (Life technologies). cDNAs of serine hydrolase genes were amplified by specific primer sets (**Table 1**). cDNAs of mouse PNPLA6 (NM_001122818) and mouse PNPLA7 (NM_144738) were provided from Dr. Rudolf Zechner (University of Graz, Austria, Kienesberger *et al.*, 2008). Obtained cDNAs for mouse or rat serine hydrolase genes were subcloned into pCAGGS-Flag (N), pCAGGS-HA(N), and pEGFP-N. All PCR products were analyzed by DNA sequencing (3130xl Genetic Analyzer, Life technologies; Functional Genomics Facility, National Institute

for Basic Biology).

Mutagenesis

Mouse ABHD17B S170A, D235A and H264A mutants were generated by site-directed mutagenesis using the following primer pairs: S170A, 5'-ATGTGATTATATATGGCCAGGCCATAGGGACAGTGCCATCTGT-3' and 5'-ACAGATGGCACTGTCCCTATGGCCTGGCCATATATAATCACAT-3'; D235A, 5'-ATTAATAATTCACGGGACTGAAGCTGAAGTCATTGACTTTTCCCATG-3' and 5'-CATGGGAAAAGTCAATGACTTCAGCTTCAGTCCCGTGAATTATTAAT-3'; and H264A,

5'-CCTGTGGGTTGAAGGGGCAGGAGCCAATGACGTGGAGCTTTATGGAC-3' and 5'-GTCCATAAAGCTCCACGTCATTGGCTCCTGCCCCTTCAACCCACAGG-3'

(changed nucleotides are underlined). Palmitoylation-deficient ABHD17B (5CS, mouse ABHD17B C10/11/14/15/18S) was generated by PCR using the following forward primer,

5'-GCTAAGATCTACCATGAATAATCTGTCATTTAGTGAGCTATCTTCCCTCTTCTC
CTCTCCACCTTCCCCAGGGAAAATTGCTTCAAACTAG-3' (changed nucleotides are

underlined). *N*-myristoylated ABHD17B [*N*-myr, Src(1-20)/ABHD17B(21-288)] was generated by PCR using the following forward primer,

5'-GCTAAGATCTACCATGGGTAGCAACAAGAGCAAGCCCAAGGATGCCAGCCAG
CGGCGCCGCAGCCTGGAGCCCCAAAATTGCTTCAAACTAGCATTCTTGCC-3' [an

underline corresponds to mouse Src (1-60 bp)]. The resultant cDNAs were subcloned into pCAGGS-Flag (N) and pEGFP-N2. Rat PSD-95 wild-type (WT), C3L, C5L, and C3/5S mutants were generated by PCR using pGW:PSD-95-GFP as a template and the following forward primers,

5'-GCTAGAATTCACCATGGACTGTCTCTGTATAGTGACAACCAAGAAATA-3'

5'-GCTAGAATTCACCATGGACTTTACTCTGTATAGTGACAACCAAGAAATA-3',

5'-GCTAGAATTCACCATGGACTGTCTCTTTAATAGTGACAACCAAGAAATA-3', and

5'-GCTAGAATTCACCATGGACTCTCTCTCTATAGTGACAACCAAGAAATA-3',

respectively (changed nucleotides are underlined). The reverse primer 5'-GCTAGCGGCCGCTCAGAGTCTCTCTCGGGCTGGGACC-3' was used for all PSD-95 constructs. The resultant cDNAs were subcloned into pCAGGS. Mouse Hras WT cDNA was cut out from pEGFP-C:Hras and subcloned into pCAGGS-Flag (C). Hras C181S, C184S, and C181/184S mutants were generated by PCR using pCAGGS:Flag-Hras as a template, the forward primer 5'-GCTAGGATCCACCATGACAGAATACAAGCTTGTGGTGG-3', and the following reverse primers:

5'-GCTAGGATCCTCAGGACAGCACACATTTGCAGCTCATGGAGCCAGGACCACTCTCATCGG-3',

5'-GCTAGGATCCTCAGGACAGCACACATTTGGAGGCTCATGCAGCCAGGACCCTCTCATCGG-3', and

5'-GCTAGGATCCTCAGGACAGCACACATTTGGAGGCTCATGGAGCCAGGACCACTCTCATCGG-3',

TCATCGG-3', respectively (changed nucleotides are underlined). The resultant cDNAs were subcloned into pCAGGS-Flag(C).

Cell culture and transfection

HEK293T cells

HEK293T cells were grown in Dulbecco's Modified Eagle Medium (DMEM, Sigma-Aldrich) supplemented with 10% fetal bovine serum (FBS, Sigma-Aldrich) at 37°C with 5% CO₂. After 14-20 hours, HEK293T cells were transfected with plasmid DNAs by Lipofectamine and plus reagent system (Life technologies).

Cultured rat hippocampal neurons

Hippocampi were dissected from E18-19 embryonic rats (Wistar/ST, Japan SLC, Shizuoka, Japan) and treated in Hank's buffered saline (Sigma-Aldrich) with 10 U/ml papain (Worthington Biochemical Corp., Lakewood, NJ) and DNase I (Sigma-Aldrich) for 10 min at 37°C. To titrate the papain activity, reaction solution was diluted by equal volume of ice-cold horse serum (Life technologies). Hippocampi were triturated and cells were collected by centrifugation at 1,000 x g for 5 min at 4°C. Cells were washed twice with trituration and centrifugation, suspended in neurobasal medium (Life technologies) containing 10% FBS, filtrated with 70 µm cell strainer (BD Falcon, Franklin Lake, NJ), and plated on poly-L-lysine (Sigma-Aldrich)-coated cover slips (Matsunami, Osaka, Japan) at a density of 5.0 x 10⁵ cells

per well (6-well plate), 2.5×10^5 cells per well (12-well), and 2.5×10^4 cells per well (24-well). Three hours later, the medium was replaced with neurobasal medium supplemented with B-27 supplement (Life technologies) and 2 mM Glutamax (Life technologies). Cells were cultured at 37°C with 5% CO₂. Fresh medium was added after 7 days *in vitro* (DIV) and half of medium was changed weekly thereafter. Cultured neurons were transfected with plasmid DNAs by Lipofectamine 2000 (Life technologies).

Adeno-associated virus (AAV) vectors

Construction of microRNA vectors for AAV generation

MicroRNAs (miR/miRNA) were prepared by BLOCK-iT RNAi Pol II miR RNAi system (Life technologies). miRNAs were designed by BLOCK-iT RNAi Designer (Life technologies home page, <https://rnaidesigner.lifetechnologies.com/rnaiexpress/>). Top and bottom single-strand oligo DNAs were annealed to generate double-strand DNAs and subcloned into pcDNA6.2:EmGFP-miRNA vector according to the manufacture's instruction. To prepare AAV vectors, pre-miRNA expression cassette of pcDNA6.2:EmGFP-miRNA was subcloned into pAAV-CAGGS-MCS-WPRE vector (provided by Dr. Kenta Kobayashi, Section of Viral Vector Development, NIPS). I prepared 4-10 miRNA vectors for individual genes, validated knockdown efficiencies of miRNAs using co-transfection systems with indicated proteins in HEK293T cells, and selected the best miRNAs. Target sequences of miRNAs and top and bottom single-strand oligo DNAs used are listed in **Table 2**.

Generation of AAV vectors

DJ-type AAV (AAV-DJ) is a recently developed serotype of AAV and has high infection capacities for various cells (Grimm *et al.*, 2008). Following AAV-DJ vectors: AAV-DJ:ABHD17B-HA WT, AAV-DJ:ABHD17B-HA D235A, AAV-DJ:EmGFP-miR-lacZ, AAV-DJ:EmGFP-miR-ABHD17A, AAV-DJ:EmGFP-miR-ABHD17B, AAV-DJ:EmGFP-miR-ABHD17C, AAV-DJ:EmGFP-miR-ABHD1, AAV-DJ:EmGFP-miR-ABHD3, AAV-DJ:EmGFP-miR-ABHD4, AAV-DJ:EmGFP-miR-ABHD12, AAV-DJ:EmGFP-miR-ABHD13, AAV-DJ:EmGFP-miR-ABHD16A, AAV-DJ:EmGFP-miR-Lypla1, and AAV-DJ:EmGFP-miR-Lypla2, were generated by Dr. Kenta Kobayashi as follows. HEK293T cells were co-transfected with pAAV-DJ-RC, pAdHelper, and constructed pAAV vectors by the calcium phosphate method. AAV-DJ particles were purified from cell extracts by two times CsCl₂ density gradients. Virus genome (vg) titers were determined by real-time PCR (Yagi *et al.*, 2011).

AAV infection into neurons

AAV particles were diluted in the conditioned medium of cultured neurons. Cultured neurons (13-14 DIV) were infected with 5.0×10^4 vg/cell of AAVs. For ABHD17B-overexpression experiments, infected neurons were cultured for 5 days and subjected to the APEGS assay or

the immunoprecipitation. For miRNA-based knockdown experiments, after 6 days infection total RNA was extracted for real-time PCR. After 7 days infection cell lysates were subjected to the APEGS assay.

Acyl-PEGyl exchange gel shift (APEGS) assay

HEK293T cells or cultured neurons were washed with phosphate-buffered saline (PBS) at room temperature and solubilized with 0.125 ml of Buffer A (PBS containing 4% SDS, 5 mM EDTA, 50 µg/ml PMSF, 10 µg/ml leupeptin, and 10 µg/ml pepstatin A). Cell lysates were incubated for 10 min at 37°C, diluted with 0.375 ml (3 vol.) of Buffer B (PBS containing 5 mM EDTA, 50 µg/ml PMSF, 10 µg/ml leupeptin, and 10 µg/ml pepstatin A), and then transferred into 1.5 ml tubes. Samples were reduced with 10 mM TCEP for 30 min and alkylated with 40 mM NEM for 3 hours at room temperature with end-over-end rotation. Excess of TCEP and NEM was removed with a chloroform/methanol precipitation (CM ppt, Wessel and Flugge, 1984). Protein pellets were resuspended with 0.125 ml of Buffer A and incubated in 0.375 ml (3 vol.) of Buffer H (1.33 M hydroxylamine pH 7.0 and 5 mM EDTA) to cleave thioester bonds or Buffer T (1.33 M Tris-HCl pH 7.0 and 5 mM EDTA) as a negative control for 1 hour at 37°C without a rotation. Excess of hydroxylamine was removed with a CM ppt. Protein pellets were resuspended with 0.1 ml of Buffer C (PBS containing 2% SDS, 50 µg/ml PMSF, 10 µg/ml leupeptin, and 10 µg/ml pepstatin A). Total protein concentration was measured by bichinchoninic acid (BCA) protein assay (Thermo Fisher

scientific) and adjusted to 0.5 mg/ml with Buffer C. One hundred microlitter of samples (50 µg of total proteins) were reduced with 10 mM TCEP and then PEGylated with 20 mM mPEGs for 1 hour at room temperature with a shaker (Thermomixer, Eppendorf, Hamburg, Germany). Excess of mPEG was removed with a CM ppt. Protein pellets were resuspended with Laemmli SDS-sample buffer without reductants and boiled at 100°C for 2 min. PEGylated proteins were resolved by SDS-PAGE and analyzed by western blotting using specific antibodies for target proteins.

For the analysis of depalmitoylation processes of PSD-95 and Hras in neurons, cultured neurons were treated with 100 µM of 2-BP in the conditioned medium for the indicated time periods, washed by PBS, and subjected to the above protocol. For the investigation of ABHD17B inhibitors, mock or ABHD17B-expressing cultured neurons were treated with 100 µM of indicated inhibitors for 2 hours, washed by PBS, and subjected to the above protocol.

SDS-PAGE and western blotting

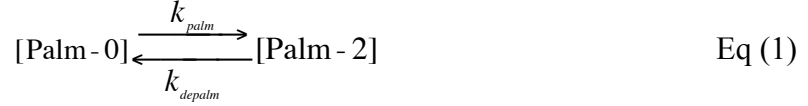
I prepared the following polyacrylamide gels: 6% gel for PSD-95 and calnexin; 10% gel for $G\alpha_q$ and $G\alpha_s$; and 14% gel for Hras, Nras, Cav1, and SNAP25. SDS-PAGE was done in the running buffer (25 mM Tris, 200 mM glycine, and 0.1% SDS). For general purpose of western blotting, the protein transfer to the polyvinylidene difluoride (PVDF) membrane of western blotting was performed by a semi-dry transfer system using TRANS BLOT SD

CELL (BIO RAD, Hercule, CA) with the transfer buffer (25 mM Tris, 200 mM glycine, and 20% methanol) at 20 V for 1 hour. Western blotting for PEGylated proteins prepared by the APEGS assay was performed with a wet transfer system (NA-1511C and power forester 3870, Nihon Eido, Tokyo, Japan) in the wet transfer buffer (50 mM Tris, 385 mM glycine, and 20% methanol) at 80 V for 4 hours with cooling at 4 °C by Neocool Circulator CF30 (Yamato Scientific., Tokyo, Japan). The membrane was then blocked with 2% skim milk (Wako pure chemical) in 0.05% Tween20-containing tris-buffered saline (TTBS) for 20 min and treated with primary antibodies diluted in 2% skim milk (1:250-2,000) in Hybri-Bags (Cosmo Bio, Tokyo, Japan) for 1-2 hours at room temperature or overnight at 4°C. Membranes were washed by TTBS for 5 min (for general experiments) or 3 min (for APEGS assays) three times and treated with secondary antibodies. After being washed, membranes were treated with ECL plus reagent (Thermo Fisher scientific) for 5 min. Chemical luminescence was detected by X-ray films RX-U or Super RX (Fuji film, Tokyo, Japan). For quantitative western blotting, the signal was captured by Light-Capture II (ATTO, Tokyo, Japan) and analyzed with CS Analyzer (ATTO).

Mathematical simulation

Steady-state palmitoylation cycle of PSD-95

Palmitate cycling on PSD-95 under the steady-state was approximated by the following equilibration.



[Palm-0] and [Palm-2] represented non-palmitoylated and di-palmitoylated PSD-95, respectively (**Figure 8A**). k_{palm} and k_{depalm} indicated rate constants of palmitoylation and depalmitoylation of PSD-95, respectively. The rate of [Palm-2] was represented by the following differential equation.

$$\frac{d[\text{Palm} - 2]}{dt} = k_{\text{palm}} [\text{Palm} - 0] - k_{\text{depalm}} [\text{Palm} - 2] \quad \text{Eq (2)}$$

Total constant was set at 100% and initial values ($t=0$) of [Palm-0] and [Palm-2] were set at $x\%$ and $(100-x)\%$, respectively. The solution of Eq (2) was represented by the following equation.

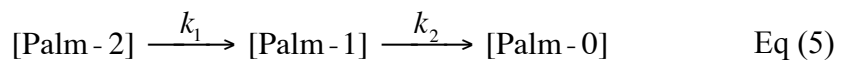
$$[\text{Palm} - 2] = \frac{100}{k_{\text{palm}} + k_{\text{depalm}}} \left[k_{\text{palm}} + \left\{ (x - 1)k_{\text{palm}} + k_{\text{depalm}}x \right\} e^{-(k_{\text{palm}} + k_{\text{depalm}})t} \right] \quad \text{Eq (3)}$$

The end point was calculated the following equation.

$$[\text{Palm} - 2]_{\infty} = \lim_{t \rightarrow \infty} [\text{Palm} - 2] = \frac{100 \times k_{\text{palm}} / k_{\text{depalm}}}{1 + k_{\text{palm}} / k_{\text{depalm}}} \quad \text{Eq (4)}$$

Step-wise depalmitoylation reaction of PSD-95

In the presence of 2-BP, the depalmitoylation process of PSD-95 could be represented by the following reactions.



[Palm-2], [Palm-1], and [Palm-0] were di-palmitoylated, mono-palmitoylated and non-palmitoylated PSD-95, respectively (**Figure 10A**). k_1 and k_2 indicated individual rate

constants. Rates of [Palm-2], [Palm-1] and [Palm-0] were represented by the following simultaneous differential equations.

$$\begin{aligned}\frac{d[\text{Palm} - 2]}{dt} &= -k_1[\text{Palm} - 2] \\ \frac{d[\text{Palm} - 1]}{dt} &= k_1[\text{Palm} - 2] - k_2[\text{Palm} - 1] \\ \frac{d[\text{Palm} - 0]}{dt} &= k_2[\text{Palm} - 1]\end{aligned}\quad \text{Eq (6)}$$

Total constant was set at 100% and initial values ($t=0$) of [Palm-2], [Palm-1] and [Palm-0] were set at $x\%$, $y\%$ and $(100-x-y)\%$, respectively. The solutions of Eq (6) were represented by the following equation.

$$\begin{aligned}[\text{Palm} - 2] &= 100xe^{-k_1t} \\ [\text{Palm} - 1] &= \frac{100}{k_2 - k_1} \left[k_1xe^{-k_1t} + \{k_2y - k_1(x + y)\}e^{-k_2t} \right] \\ [\text{Palm} - 0] &= 100(1 - [\text{Palm} - 2] - [\text{Palm} - 1])\end{aligned}\quad \text{Eq (7)}$$

All calculations were done by Microsoft Excel software.

Metabolic [^3H]-palmitate labeling assay

HEK293T cells (2.5×10^5 cells) were seeded in 12 well-plates. Cells were co-transfected PSD-95-GFP WT or C3/5S with individual serine hydrolase clones. After 24 hours, cells were preincubated for 30 min in serum-free DMEM with fatty acid-free bovine serum albumin (BSA, final concentration 5 mg/ml, Sigma-Aldrich). Then, cells were labeled with 0.25 mCi/ml [^3H]-palmitate (Perkin Elmer Japan, Yokohama, Japan) for 4 hours in the preincubation medium. Cells were washed with PBS at room temperature, lysed by 0.5 ml of SDS-PAGE sample buffer (62.5 mM Tris-HCl pH 6.8, 10% glycerol, 2% SDS, 0.001%

bromophenol blue, and 10 mM dithiothreitol), and boiled at 90°C for 2 min. For fluorography, proteins were separated by SDS-PAGE. Gels were fixed by the fixation solution (25% isopropanol and 10% acetic acid) for 20 min. Then gels were treated with the fluorography solution (1 M sodium salicylate and 15% ethanol) for 20 min to amplify the radioisotope signal. After gel drying, gels were exposed to X-ray films RX-U at -80°C. Quantitative analysis of fluorography was performed by Image J software (NIH image). For coomassie brilliant blue (CBB) staining, proteins were separated by SDS-PAGE, transferred to membranes, and stained by CBB-R250 (Wako pure chemical).

***In silico* structural predictions and sequence alignments**

In silico structural predictions and modeling were performed by the online free software, HH-pred run by Max-Planck Institute for Developmental Biology (<http://toolkit.tuebingen.mpg.de/hhpred>, Soding *et al.*, 2005). Sequence alignments were performed by Clustal W2 run by European Molecular Biology Laboratory (<http://www.ebi.ac.uk/Tools/msa/clustalw2>, Larkin *et al.*, 2007). The phylogenetic tree (**Figure 12**) was generated by Sea View distributed by PRABI-Doua (Gouy *et al.*, 2010).

Immunofluorescence analysis and fluorescence microscopy

For GFP-fusion proteins, transfected cultured neurons (2.5 x 10⁴ cells in 24-well plate; 21-24 DIV) were fixed with 4% paraformaldehyde/120 mM sucrose/100 mM

4-(2-hydroxyethyl)-1-piperazine ethane sulfonic acid (HEPES) pH 7.4 at room temperature for 10 min. For staining of total PSD-95 and palmitoylated PSD-95, neurons were fixed with methanol at -30°C for 10 min and blocked with 1% BSA for 10 min on ice. Total PSD-95, palmitoylated PSD-95, and HA-tagged proteins were detected by anti-PSD-95 (clone 7E3-1B8), hPF11 (Fukata *et al.*, 2013) and anti-HA (clone 3F10) antibodies. Then, neurons were visualized with Alexa Fluor 647-conjugated anti-mouse IgG, DyLight 488-conjugated anti-human IgG Fc, and Cy3-conjugated anti-rat IgG secondary antibodies. Fluorescent images were acquired with a confocal laser scanning microscopy system (TCS SP5 II; Leica, Wetzlar, Germany) equipped with an HCXPL APO 63x/1.40 oil immersion objective lens, combined with the Leica HyD detector.

Immunoprecipitation (IP)

Cultured neurons (5×10^5 cells in 6-well plate; 13-14 DIV) were infected with AAV-DJ:EmGFP-miR-lacZ (for a mock), AAV-DJ:ABHD17B-HA WT, or D235A. After 5 days, cells were treated by RIPA buffer [50 mM Tris-HCl (pH 8.0), 150 mM NaCl, 1% IgepalCA-630 (Sigma-Aldrich), 0.5% deoxycholate (Sigma-Aldrich), 0.1% SDS, and 50 µg/ml PMSF] for 20 min on ice. Collected cell lysates were clarified by the centrifugation at 11,000 x g for 10 min and supernatants were incubated with 15 µg of anti-HA antibody (12CA5) for 1 hour. Then, protein A-Sepharose (GE healthcare) was added and this mixture was incubated for 1 hour. After being washed with Buffer W (20 mM Tris-HCl pH 7.4, 1 mM

EDTA, 100 mM NaCl, and 1% TritonX100) six times, precipitated beads were treated with 150 μ l of Laemmli SDS-sample buffer with 2% 2-mercaptoethanol and boiled at 100 °C for 5 min.

Real-time quantitative PCR

Total RNA of cultured hippocampal neurons was extracted by the Trizol method (see section of Cloning of serine hydrolase genes and plasmid construction). cDNA was synthesized using the High-Capacity cDNA RT kit (Life technologies). Real-time PCR was performed using an Applied Biosystems StepOnePlus™ Real-Time PCR System (Life technologies) and SYBR Green PCR Fast Master Mix (Life technologies). I used two independent primer pairs for individual target genes (**Table 3**). 100 nM of primer pairs and 10 ng of synthesized cDNA were used for the reaction. For the absolute quantification, a set of standard template samples were prepared as follows. The individual full-length target cDNAs were cut out from pCAGGS constructs and purified by the agarose gel electrophoresis and the QIAquick spin column (QIAGEN, Valencia, CA). Concentrations of standard cDNAs were measured with NanoDrop2000 [Thermo Fischer scientific, kindly shared with us by Tominaga Laboratory (NIPS)]. Dilution series for standard cDNAs were prepared by diluting with salmon sperm DNA fragment (10 μ g/ml, Life technologies). For the relative quantification, GAPDH was used as an internal control and expression levels were estimated by the $\Delta\Delta C_t$ method.

Results

Chapter 1

Development of a novel quantitative method for *S*-palmitoylation

Contents

1. Principle of a novel quantitative APEGS assay	35
2. Selection of mPEGs	36
3. Optimization of reaction conditions	37
4. Mobility shifts depend on the number of <i>S</i> -palmitoylation	39
5. The number of sites and stoichiometry of various neuronal <i>S</i> -palmitoylated proteins	40
6. Mathematical modeling of the palmitate cycling on PSD-95	42
7. Monitoring of depalmitoylating processes of PSD-95 and Hras by the APEGS assay	43
8. Mathematical simulation of the depalmitoylation process of PSD-95	43

1. Principle of a novel quantitative APEGs assay

Although recent palmitoyl-proteome analysis identified a substantial number of palmitoyl proteins (Kang *et al.*, 2008; Martin and Cravatt, 2009; Yang *et al.*, 2010; Martin *et al.*, 2011), no methods have addressed the number of palmitoylated cysteine residues in proteins and their palmitoylation stoichiometries *in vivo*. Here, I assumed that if a reversible thioester linkage on a palmitoylated protein can be specifically exchanged with some high-molecular weight moieties, mobility shifts of the target protein on SDS-PAGE should reflect the number of palmitoylated cysteine residues. To examine my hypothesis, I chose polyethylene glycols (PEGs) with defined molecular masses, because similar mass-tagging strategies using PEGs, so called PEG-switch were reported in cysteine oxidation (Makmura *et al.*, 2001; Burgoyne *et al.*, 2013) and in *O*-glycosylation (Rexach *et al.*, 2010). My method comprises sequential four chemical steps which combined principles of ABE method and PEG-switch (**Figure 1**): 1) reduction of intra- and intermolecular disulfide bonds by TCEP (Yang *et al.*, 2010); 2) blockade of free cysteine thiols with NEM (Wan *et al.*, 2007); 3) hydroxylamine treatment to cleave palmitoyl-cysteine thioester linkages (Magee *et al.*, 1984); and 4) introduction of maleimide-conjugated PEGs (mPEGs) into newly exposed cysteine thiols (*S*-PEGylation), which are originally *S*-palmitoylated cysteines. *S*-PEGylated proteins should show mobility shifts on SDS-PAGE depending on the number of incorporated PEGs and reflect the occupancy of their palmitoyl cysteines (**Figure 1**). This method simultaneously detects the band of non-palmitoylated target protein without any mobility shifts. This method would

provide important information by measuring the relative intensities of palmitoylated and non-palmitoylated protein bands: 1) the palmitoylation stoichiometry (*i.e.*, the palmitoylation levels in cells, tissues, or any samples) and 2) the ratio of the individual palmitoylation states (*i.e.*, mono-, di-, or multiply palmitoylated). Thereafter, I refer to this method as an acyl-PEGyl exchange gel shift (APEGs) assay.

2. Selection of mPEGs

To determine the optimal mPEG molecular size that predictably affects the protein mobility in the APEGs assay, I first applied four different mPEGs [average molecular weights, 1,000 (1k), 2,000 (2k), 5,000 (5k), and 10,000 (10k) g/mol] to the APEGs assay for three palmitoyl proteins with different molecular weight, Hras (21 kDa), G α_q (42 kDa), and PSD-95 (95 kDa) (**Figure 2**). These proteins are all shown to have two palmitoyl cysteines and expected to be highly palmitoylated in neurons judging from their predominant plasma membrane/synaptic localization (Hancock *et al.*, 1989; Wedegaertner *et al.*, 1993; Topinka and Brett, 1998; Tsutsumi *et al.*, 2009). Reaction of cell lysates from hippocampal neurons with mPEG-1k and -2k produced a single band of Hras, respectively, with different mobility shifts from the original position, consistent with incorporation of two PEG moieties (**Figure 2A**). However, mPEG-1k reaction did not induce apparent mobility shifts of G α_q and PSD-95 (**Figure 2B, C**). mPEG-2k reaction produced three clearly separated bands of G α_q corresponding to non-, mono-, and di-PEGylated G α_q (**Figure 2B**) but was still not suitable to induce mobility shifts

of PSD-95 (**Figure 2C**). mPEG-5k reaction produced two bands of PSD-95, an upper major band and a lower faint band for non-PEGylated PSD-95 at the original position (**Figure 2C**). In contrast, mPEG-5k- or mPEG-10k-modified Hras and G α_q and mPEG-10k-modified PSD-95 were not detectable by western blotting. These results suggest that selection of proper molecular size of mPEG is very important to obtain precise results. I selected mPEG-2k and mPEG-5k for <60 kDa and >60 kDa proteins, respectively.

3. Optimization of reaction conditions

To precisely quantify *S*-palmitoylation stoichiometries, it is essential to accomplish individual reactions of the APEGS assay to saturable levels. For this purpose, I optimized the conditions for the following reactions: step 2, NEM treatment; step 3, hydroxylamine treatment; and step 4, introduction of mPEGs (**Figure 1**), using PSD-95 and Hras as di-palmitoyl model substrates (Topinka and Brecht, 1998; Hancock *et al.*, 1989). Cultured neuron lysates (0.3-0.4 mg/ml total proteins) were used for each optimization. I first optimized the doses and reaction time for the NEM treatment (step 2, **Figure 3**). In the absence or low concentration (1 mM) of NEM, there were no or hardly detectable bands for both Hras and PSD-95. Under the experimental conditions, free cysteine thiols were insufficiently blocked at the step 2 and most of them could be then PEGylated irrespective of palmitoylation, resulting in protein loss during the CM ppt step and western blotting probably due to the highly hydrophilic nature of PEGs. In addition, in the condition of hydroxylamine (-), band shifts irrelevant to

palmitoylation were observed with less than 10 mM NEM, indicating that at least 20 mM of NEM was required to completely block free cysteine thiols at the step 2 (**Figure 3A**). I also found that NEM incubation over 1 hour is necessary for complete blocking as the intermediate product (mono-palmitoylated PSD-95) appeared in 0.5-hour incubation (**Figure 3B**, left panel). I concluded that 40 mM NEM treatment for 3 hours is sufficient to completely block free cysteine thiols at the step 2.

Next, I optimized doses for the hydroxylamine treatment (step 3, **Figure 4**). A previous study reported that a treatment with 1 M hydroxylamine efficiently removes palmitates from proteins (Magee *et al.*, 1984). When I examined the dose-dependency of hydroxylamine treatment, over 0.5 M was sufficient to release palmitates from the two palmitoylated cysteine residues of both PSD-95 and Hras (**Figure 4**). I noted that the treatment with over 1.25 M hydroxylamine precipitated proteins and caused the loss of proteins during the reaction, probably due to the salting out by the high concentration of salt. Then, I selected the conventional condition (1 M hydroxylamine, pH 7.0 for 1 hour) as an optimal deacylation condition of the APEGS assay.

Then, I optimized the reaction condition in the PEGylation step (step 4, **Figure 5**). For 0.5 mg/ml total proteins, treatment with over 10 mM mPEG-5k provided saturable reactions (about 80% of di-palmitoylated PSD-95, **Figure 5A**). I noted that mono-PEGylated PSD-95

was detected together with small amount of di-PEGylated PSD-95 under 5 mM mPEG-5k condition, indicating the significance of optimization of mPEG doses to obtain precise stoichiometries of *S*-palmitoylated proteins. When I checked optimal total protein concentration used for the reaction under the 20 mM mPEG-5k condition, all points from 0.3 to 1.5 mg/ml total proteins showed similar PEGylation patterns (**Figure 5B**). Subsequently, I investigated optimal reaction time of PEGylation and found that PEGylation was completed within 10 min (**Figure 5C**). Taken together, I concluded that 20 mM mPEGs treatment for 1 hour is sufficient to obtain saturable reactions for precise quantification.

4. Mobility shifts depend on the number of *S*-palmitoylation

To validate whether mobility shifts observed in the APEGS assay actually depend on the number of *S*-palmitoylation, I prepared a series of palmitoylation-deficient mutants of PSD-95 and Hras (**Figure 6**). El-Husseini *et al.* reported that PSD-95 C3L and PSD-95 C5L mutants are mono-palmitoylated and that PSD-95 C3/5S is not palmitoylated (El-Husseini *et al.*, 2000b). Roy *et al.* reported that Hras C181S and Hras C184S mutants are mono-palmitoylated and that Hras C181/184S is not palmitoylated (Roy *et al.*, 2005). Wild-type (WT) and mutants were expressed in HEK293T cells and the cell lysates were subjected to the APEGS assay. In the case of PSD-95, PSD-95 proteins were co-expressed with DHHC3 to increase palmitoylation levels. Consistently, I found that PSD-95 WT showed two-step mobility shifts, that C3L and C5L had the only one-step mobility shift, and that C3/5S did not show any

mobility shifts (**Figure 6A**). Hras showed similar patterns to PSD-95 (**Figure 6B**). These results indicate that mobility shifts of PSD-95 and Hras in the APEGS assay reflect the number of their *S*-palmitoylation.

5. The number of sites and stoichiometry of various neuronal *S*-palmitoylated proteins

Taking advantage of the APEGS assay, I attempted to verify the number and stoichiometry of *S*-palmitoylation of various endogenous proteins in cultured rat hippocampal neurons. I chose PSD-95, calnexin, Hras, Nras, $G\alpha_s$, $G\alpha_q$, caveolin1 (Cav1), and SNAP25 as representative *S*-palmitoylated proteins because these proteins are well-characterized *in vitro* in terms of their palmitoylation sites (**Figure 7**). To see whether the observed band shifts are specifically attributed to the palmitoylated cysteines, I performed APEGS assay with or without hydroxylamine treatment at the step 3. In addition, I confirmed that omission of mPEG from the reaction at the step 4 prevented any mobility shifts for all the protein tested (**Figure 1**). I found that about 80% of PSD-95 was di-palmitoylated and that mono-palmitoylated form of PSD-95 was hardly detected in cultured hippocampal neurons (**Figure 7A, I**). I could detect a band of mono-PEGylated PSD-95 in an overexposed film (data not shown). Calnexin, an endoplasmic reticulum (ER) resident membrane protein, was reported to have two palmitoyl cysteines (Lakkaraju *et al.*, 2012). Consistently, I detected two slow-migrating bands and found that the stoichiometry of calnexin palmitoylation was almost 100% and that it mostly existed as a di-palmitoylated form (**Figure 7B, I**). Hras and Nras have two and one palmitoyl

cysteine residues, respectively (Hancock *et al.*, 1989). Fitting with this, Hras had two-step mobility shifts and Nras showed one-step mobility shift (**Figure 7C, D, I**). Trimeric G protein α subunits $G\alpha_s$ and $G\alpha_q$ have one and two palmitoyl cysteine residues, respectively (Wedegaerther *et al.*, 1993). $G\alpha_s$ and $G\alpha_q$ showed one- and two-step band shifts, respectively (**Figure 7E, F, I**). Cav1 has three palmitoyl cysteines, C133, C143 and C156 (Dietzen *et al.*, 1995). PEGylation generated three slow-migrating bands (**Figure 7G**), suggesting that a major palmitoylated form of Cav1 is di-palmitoylated form and that Cav1 exists as a heterogenous mixture of various palmitoylated forms in neurons (**Figure 7G, I**). SNAP25 that has four putative palmitoylation sites (Gonzalo and Linder, 1998; Greaves *et al.*, 2009) showed non-specific band shifts even without the hydroxylamine treatment (**Figure 7H**). I also observed a similar pattern in AMPA type glutamate receptor subunit GluA1 (data not shown). I reasoned that some specific structures, for example cysteine rich polypeptides and transmembrane structures, would cause insufficient blocking of free cysteine thiols by NEM. Thus, this approach can be applicable to many endogenous palmitoylated proteins with simultaneous assessment of specificity of mobility shifts. I calculated distances of mobility shifts of proteins tested here in **Table 4** and I noted that actual migration distances did not always correspond to 2 kDa or 5 kDa of mPEG used and differed between proteins. I detected minor bands, such as mono-PEGylated PSD-95, using overexposed data (data not shown). These results represent the first and direct demonstration of *S*-palmitoylation stoichiometries of endogenous proteins and, in addition, their *in vivo* *S*-palmitoylation states (*i.e.*, mono-, di-,

tri-, and more).

6. Mathematical modeling of the palmitate cycling on PSD-95

To explore the physiological meaning of the obtained stoichiometry of *in vivo* PSD-95 palmitoylation, I constructed a mathematical simulation model. Because about 80% of PSD-95 was di-palmitoylated and little PSD-95 was mono-palmitoylated in the basal state of neurons (**Figure 7A, I**), I approximated the palmitate cycling on PSD-95 to the reversible first-order reaction between di-palmitoylated [Palm-2] and non-palmitoylated [Palm-0] forms [Eq (1) in Materials and Methods, **Figure 8A**]. I set [Palm-2] and [Palm-0] at 80% and 20%, respectively, explored k_{palm}/k_{depalm} to meet the setting values using Eq (4) in Materials and Methods, and obtained the rate constant ratio k_{palm}/k_{depalm} to be 4 (**Figure 8B**). This result indicates that the palmitoylation reaction of PSD-95 catalyzed by DHHC PATs would be about 4 times as fast as the depalmitoylation reaction mediated by unknown depalmitoylating enzyme(s) in the resting neurons. Subsequently, I investigated the effect of changes in PAT or PPT activities on the PSD-95 palmitoylation state (**Figure 8C, D**). It was predicted that inhibition of PAT activity causes relatively slow changes in PSD-95 palmitoylation levels (**Figure 8C**). In contrast, increase of PPT activity would more rapidly reduce the level of PSD-95 palmitoylation (**Figure 8D**). These simulations strongly suggest that PATs mainly keep the PSD-95 palmitoylation at high levels and depalmitoylating enzyme(s) may rapidly downregulate the palmitoylation levels of PSD-95 upon extracellular stimuli such as

glutamate.

7. Monitoring of depalmitoylating processes of PSD-95 and Hras by the APEGS assay

So far, the half-life of palmitate on PSD-95 was shown to be approximately 2 hours by an [¹²⁵I]-palmitate pulse-chase experiment (El-Husseini *et al.*, 2002), although the detailed processes, dynamic changes between two palmitoylated states, remain unclear. Here, I assumed that the quantitative APEGS assay allows me to dissect the PSD-95 depalmitoylation process in more details. To extract the depalmitoylation process, I used 2-bromopalmitate (2-BP), a potent irreversible inhibitor of palmitoylating enzymes (Webb *et al.*, 2000; Davda *et al.*, 2013). When cultured rat hippocampal neurons were treated with 2-BP, the amount of di-palmitoylated PSD-95 was gradually reduced over time and reciprocally that of non-palmitoylated PSD-95 was increased (**Figure 9A, C**). Importantly, I could not see the mono-palmitoylated PSD-95 at any time points during the 2-BP treatment. The half-life of di-palmitoylated PSD-95 was calculated to be 1.84 ± 0.46 hours (**Figure 9E**), very consistent with previous pulse-chase experiment (El-Husseini *et al.*, 2002). In contrast, the depalmitoylation process of Hras was much slower than that of PSD-95 in neurons (**Figure 9B, D**).

8. Mathematical simulation of the depalmitoylation process of PSD-95

Previous section showed that PSD-95 was rapidly depalmitoylated in cultured neurons in the

presence of 2-BP. To discuss the depalmitoylation process of PSD-95, I constructed a mathematical simulation of the 2-step sequential depalmitoylation process [Eq(5) in Materials and Methods, **Figure 10A**]: k_1 and k_2 represent rate constants for the first and second depalmitoylation steps, respectively. I input experimental initial values from **Figure 9A** and **C**: $[\text{Palm-2}]_{t=0}=77\%$, $[\text{Palm-1}]_{t=0}=8\%$, and $[\text{Palm-2}]_{t=0}=15\%$, into Eq (7) in Materials and Methods, and screened various ratios of k_1/k_2 . **Figure 10B-H** showed predicted patterns of the 2-step simulation given various k_1/k_2 values. Among these simulations, the simulation (**Figure 10F**, $k_1/k_2=0.1$) clearly reproduced the experimental pattern (**Figure 9C**), in which there were no detectable products of mono-palmitoylated PSD-95 during the depalmitoylation process of di-palmitoylated PSD-95. This result indicates that the second step of depalmitoylation is about 10-fold faster than the first step of depalmitoylation, suggesting that two palmitoyl-cysteine residues are cleaved almost simultaneously by depalmitoylating enzyme(s).

Chapter 2

Exploration of novel depalmitoylating enzymes for PSD-95

Contents

1. Screening for PSD-95 palmitoyl-protein thioesterases (P-PPTs)	46
2. P-PPT candidate genes are expressed in hippocampal neurons	48
3. ABHD17 subfamily members are localized in dendritic spines	48
4. Identification of the catalytic triad of ABHD17 subfamily members	48
5. ABHD17B specifically reduces the palmitoylation level of PSD-95 in neurons	49
6. ABHD17B directly interacts with PSD-95	50
7. Localization and function of ABHD17B are regulated by its N-terminal palmitoylation	51
8. Treatment with palmostatin-B inhibits an enzymatic activity of ABHD17B	52
9. Knockdown of P-PPT candidates dose not inhibit the depalmitoylation of PSD-95	53

1. Screening for PSD-95 palmitoyl-protein thioesterases (P-PPTs)

Although S-palmitoylation is one of the most common “reversible post-translational modifications”, the enzymes that mediate depalmitoylation have been controversial over 35 years. Identifying these enzymes is a long-standing question. So far, four enzymes, Lypla1 (Duncan and Gilman, 1998), Lypla2 (Tomatis *et al.*, 2010), Lyplal1 (Tian *et al.*, 2012), and PPT1 (Camp and Hofmann, 1993), have been reported as depalmitoylating enzymes by *in vitro* reconstitutions or by overexpression experiments. However, their physiological roles remain unclear. Martin *et al.* recently showed that hexadecylfluorophosphonate (HDFP), an inhibitor of broad serine hydrolases, inhibits depalmitoylation processes of several palmitoylated proteins such as Nras, G α_q and MPPs (members of the MAGUK family, Martin *et al.*, 2011). Taken together with the fact that thioesterases mainly belong to serine hydrolase superfamily, including protease, esterases, and lipases (Cantu *et al.*, 2010), I assumed that a subset of functionally uncharacterized serine hydrolases might function as depalmitoylating enzymes. Here, to identify PSD-95 palmitoyl-protein thioesterases (P-PPTs; *i.e.*, PSD-95 depalmitoylating enzymes), I isolated cDNAs of classical PPT candidates (Lypla1/2, Lyplal1, and PPT1/2) and 18 HDFP-sensitive serine hydrolases (Martin *et al.*, 2011) (**Table 1**). Most of these proteins (18/22 proteins) are deposited in the database of α/β hydrolase fold proteins (ESTHER database, Lenfant *et al.*, 2012). Furthermore, Lypla1, Lyplal1, and PPT1 are experimentally shown to have the α/β hydrolase fold (Bellizzi *et al.*, 2000; Devedjiev *et al.*, 2000; Burger *et al.*, 2012). The α/β hydrolase fold is one of the most important core domain

for serine hydrolase activities (Nardini and Dijkstra, 1999). To more widely explore P-PPTs, I additionally isolated cDNAs of 13 α/β hydrolase domain-containing (ABHD) family members that are functionally uncharacterized (Lord *et al.*, 2013) (**Table 1**, this work was done together with Mr. Tatsuro Murakami, SOKENDAI). I first examined effects of candidate proteins on the palmitoylation level of PSD-95 by a metabolic labeling assay with [³H]-palmitate in HEK293T cells. When PSD-95-GFP was expressed, [³H]-palmitate was efficiently incorporated into PSD-95-GFP (**Figure 11A**, the third lane). Under the experimental condition, the co-expression of several clones dramatically reduced palmitoylation levels of PSD-95-GFP (**Figure 11A, B**). Then, I set a threshold at 60% palmitoylation of the control for depalmitoylation activities and obtained 10 genes, ABHD1, 3, 4, 13, 16A, 17A, 17B, 17C, Lypla1, and Lypla2, as initial candidates for P-PPTs (**Figure 11B**). Especially, ABHD17A and 17B showed great depalmitoylation activities to PSD-95. To further examine the functional similarity of these candidate proteins, I generated the phylogenetic tree of α/β hydrolase fold regions of P-PPT candidates and ABHD family members as most P-PPT candidates were ABHD family members (**Figure 12, Table 5**). Based on the phylogenetic tree, I found that candidate P-PPTs can be classified into several subfamilies: ABHD1/2/3/15 subfamily (purple), ABHD4/5 subfamily (blue), ABHD12/13 subfamily (orange), ABHD16A/B (green), ABHD17A/B/C subfamily (magenta), and Lypla subfamily (yellow). ABHD5 and ABHD15 lack catalytic serine residues (Lord *et al.*, 2013), indicating that they could not function as hydrolysis enzymes.

2. P-PPT candidate genes are expressed in hippocampal neurons

To investigate mRNA expression levels of P-PPT candidates and their subfamily members (ABHD2, 12, and 16B) in cultured rat hippocampal neurons, I conducted the absolute quantification of individual mRNAs using real-time quantitative PCR. I used two independent primer sets that recognized different regions of target genes (**Table 3**). I found that all mRNAs except for ABHD16B were expressed in cultured hippocampal neurons and that ABHD17A and Lypla2 were predominantly expressed (**Figure 13**).

3. ABHD17 subfamily members are localized in dendritic spines

I next investigated subcellular localizations of GFP-fused P-PPT proteins in rat hippocampal neurons (**Figure 14**). ABHD1, 3, 13, and 16A were mainly localized in endomembranes, ABHD4 in the cytoplasm, and Lypla1/2 at the Golgi apparatus and the in cytoplasm. Importantly, ABHD17 subfamily members were uniquely localized in dendritic vesicles and dendritic spines. Because PSD-95 is depalmitoylated mainly at post-synaptic membranes (Fukata *et al.*, 2013), I focused on the post-synaptic resident ABHD17 subfamily as post-synaptic P-PPT candidates hereafter.

4. Identification of the catalytic triad of ABHD17 subfamily members

So far, no enzymatic activities of ABHD17s have been reported. To examine whether

ABHD17s have hydrolase activities, I first explored catalytic amino acids of mouse ABHD17B, the shortest form of ABHD17 subfamily members. The canonical α/β hydrolase fold generally contains the catalytic triad, Ser, Asp, and His residues, and the catalytic serine residue is conserved in Gly-Xaa-Ser-Xaa-Gly motif (Xaa is any amino acids) (Nardini and Dijkstra, 1999). Based on this consensus motif, I identified Ser170 as a candidate residue (**Figure 15A**). Because the prediction of the catalytic Asp and His is usually impossible from the primary amino acid sequence, I predicted the three dimensional structure of full-length ABHD17B using the *in silico* homology-modeling software HH-Pred and found that Asp235 and His264 of ABHD17B are located close to Ser170 on tops of loops between β -sheet and α helix in the α/β hydrolase fold (**Figure 15A, B**). To verify my predictions, I constructed point mutants in which predicted residues are replaced with alanine. All ABHD17B mutants lost the activity to reduce the level of PSD-95 palmitoylation in HEK293T cells, indicating that ABHD17B functions as a serine hydrolase with the catalytic triad, Ser170, Asp235, and His264 (**Figure 15C**). Sequence alignments of ABHD17A, B and C showed that catalytic triad amino acids were all conserved among ABHD17 subfamily members (**Figure 15D**). These results strongly suggest that ABHD17 subfamily members are enzymes that reduce the palmitoylation level of PSD-95.

5. ABHD17B specifically reduces the palmitoylation level of PSD-95 in neurons

Next, I investigated the function of ABHD17B in neurons. To ectopically overexpress

ABHD17B with high efficiency in neurons, I took advantage of AAV vectors and the effect of ABHD17B overexpression on the level of endogenous PSD-95 palmitoylation was examined by my developed APEGs assay (**Figure 16A**). When C-terminal HA-tagged ABHD17B (ABHD17B-HA) WT was overexpressed in rat hippocampal neurons, the amount of di-palmitoylated PSD-95 was robustly reduced and that of non-palmitoylated PSD-95 was increased (**Figure 16A**). This effect of ABHD17B specifically depended on its enzymatic activity because the overexpression of ABHD17B D235A did not affect the level of PSD-95 palmitoylation. In addition, the effect of ABHD17B was specific to PSD-95 as palmitoylation levels of Hras and G α_q were not changed by the expression of ABHD17B. I also investigated the effect of ABHD17B on post-synaptic clusters of PSD-95. Total PSD-95 and palmitoylated PSD-95 were stained with anti-PSD-95 and anti-palmitoylated PSD-95 (hPF11) antibodies (Fukata *et al.*, 2013, **Figure 16B**). When ABHD17B-HA WT but not D235A, was overexpressed in neurons, post-synaptic clusters of total and palmitoylated PSD-95 were dramatically reduced. These biochemical and cell biological results suggest that ABHD17B has depalmitoylating activity toward endogenous PSD-95 in neurons.

6. ABHD17B directly interacts with PSD-95

Next, I tried to establish the *in vitro* reconstitution assay to test whether ABHD17B directly catalyzes PSD-95 depalmitoylation. However, this was not successful as expected from previous evidence that *in vitro* reconstitution of serine hydrolases, especially lipases and

phospholipases, is generally difficult to be established (Mogensen *et al.*, 2005; and see a review by Dennis *et al.*, 2011). Instead, I tried to detect a direct binding of ABHD17B to PSD-95 as the enzyme-substrate interaction. Basically, the direct enzyme-substrate interaction is too transient to be detected, but it is shown that the catalytically inactive mutant of an enzyme would stably interact with its substrate as a substrate-trapping mutant (**Figure 17A**, see a review of substrate-trapping mutants for tyrosine phosphatases by Blancheto *et al.*, 2005). When ABHD17B-HA WT or catalytically inactive D235A was immunoprecipitated from neurons with anti-HA antibody, co-immunoprecipitation of PSD-95 was detected only with D235A (**Figure 17B**). This result strongly suggests that ABHD17B interacts with PSD-95 as an enzyme, and supports a hypothesis that ABHD17B directly acts on PSD-95 to hydrolyze its palmitoyl-thioester bonds.

7. Localization and function of ABHD17B are regulated by its N-terminal palmitoylation

Although ABHD17 members have no transmembrane domains, they were localized in dendritic spines and vesicles (**Figure 14**). A previous study reported that all members of ABHD17 subfamily are palmitoylated at their N-terminal cysteine rich region (**Figure 18A, D**) (Martin and Cravatt, 2009; in this paper ABHD17 is referred to as FAM108). To investigate roles of this palmitoylation in the localization and function of ABHD17B, I constructed a palmitoylation-deficient mutant (5CS, ABHD17B C10/11/14/15/18S) and an

N-myristoylated ABHD17B (*N*-myr), in which an N-terminal palmitoylation motif of ABHD17B was replaced with an *N*-myristoylation motif of Src kinase (**Figure 18B**). When expressed in neurons, 5CS was diffusely localized in the cytoplasm and *N*-myr was localized at the plasma membrane (**Figure 18C**). These results indicate that N-terminal palmitoylation of ABHD17B is necessary to target it to dendritic vesicles and spines.

Next, I also examined enzymatic activities of these mutants by the metabolic labeling assay in HEK293T cells (**Figure 18D**) and immunocytochemistry using hPF11 (**Figure 18E**). In the metabolic labeling assay with [³H]-palmitate, neither 5CS nor *N*-myr mutants expression reduced palmitoylation levels of PSD-95 (**Figure 18D**). In the hPF11 staining, ABHD17B WT dramatically reduced total and palmitoylated PSD-95 clusters. However, clusters of total and palmitoylated PSD-95 were remained in ABHD17B 5CS- and *N*-myr-expressing neurons as well as in catalytically inactive D235A-expressing neurons (**Figure 18E**). These results indicate that the palmitoylation of ABHD17B not only controls its subcellular localization but also regulates its enzymatic activity.

8. Treatment with palmostatin-B inhibits an enzymatic activity of ABHD17B

To explore inhibitors to block the thioesterase activity of ABHD17B, I investigated the effect of three lipase inhibitors, a lysophospholipase inhibitor palmostatin-B (Palm-B) which is a originally developed for Lypla1/2 (Dekker *et al.*, 2010), a gastric lipase inhibitor Orlistat, and

a broad lipase/phospholipase inhibitor methyl arachidonyl fluorophosphonate (MAFP) which inhibits the depalmitoylation process of Lck in T-cells (Zhang *et al.*, 2010), by the APEGS assay (**Figure 19A**). Treatment of ABHD17B-overexpressing rat hippocampal neurons with Palm-B strongly inhibited the ABHD17B-mediated reduction of the PSD-95 palmitoylation level. Orlistat showed a weak inhibitory effect on ABHD17B and MAFP did not show any effects. This result indicates that Palm-B targets ABHD17B in addition to its original targets, Lypla1 and 2 (Dekker *et al.*, 2010). Subsequently, to investigate an effect of Palm-B on the depalmitoylation process of endogenous PSD-95, neurons were treated with Palm-B in the presence of 2-BP and subjected to the APEGS assay (**Figure 19B**). Treatment with Palm-B completely inhibited the depalmitoylation process of PSD-95 observed in the presence of 2-BP, indicating that the target of Palm-B mediates PSD-95 depalmitoylation in neurons and suggesting that ABHD17B and Lypla1/2 are strong candidates for PSD-95 depalmitoylating enzymes.

9. Knockdown of P-PPT candidates dose not inhibit the depalmitoylation of PSD-95

Finally, I investigated whether ABHD17 members and other P-PPT candidates mediate depalmitoylation of endogenous PSD-95 in neurons. For this purpose, ABHD17A/B/C, ABHD12/13/16A, ABHD1/3/4 and Lypla1/2 were knocked down by multiple infections of individual miRNA-encoding AAVs in rat hippocampal neurons. Most of miRNA-encoding AAVs efficiently reduced mRNA levels of target genes (**Figure 20A**) without any significant

up-regulation of the other mRNAs (data not shown). Only miRNA for ABHD1 showed a small knockdown effect (~25% reduction in mRNA levels). Treatment with Palm-B, which was used as a positive control, completely inhibited the depalmitoylation process of PSD-95 observed in the presence of 2-BP (**Figure 20B**, lacZ+Palm-B). However, the depalmitoylation process of PSD-95 was not changed by the knockdown of ABHD17A/B/C, ABHD12/13/16A, ABHD1/3/4 or Lypla1/2 under the present experimental condition (**Figure 20B**).

Discussion

Contents

Characteristics of the APEGS assay	56
Depalmitoylation process of PSD-95	57
ABHD17s are promising candidates for PSD-95 depalmitoylating enzymes	58
Proposed reaction mechanism of ABHD17s	60
Proposed regulatory mechanism of ABHD17s	60
Conclusion	61

Characteristics of the APEGS assay

The APEGS assay I developed in this study is very powerful for the *S*-palmitoylation analysis as this method for the first time provides information about the number of *S*-palmitoylation sites and the stoichiometry of palmitoyl proteins. Here, I summarized the contrasting features of the APEGS assay and currently available methods including ABE and metabolic labeling methods (**Table 6**). As in the case of the ABE method, APEGS assay can be applied to any cell-free protein extracts (cells, tissues, or even purified proteins), whereas metabolic labeling methods require living cells. Furthermore, ABE method includes the purification step of biotinylated (*i.e.*, palmitoylated) proteins using the biotin-avidin system and under the current protocol, efficiencies of biotinylation and purification are not usually high. On the other hand, my APEGS assay simultaneously detects palmitoylated (*i.e.*, PEGylated) and non-palmitoylated proteins without any purification steps. Thus, the APEGS assay enables rapid and precise quantification of *in vivo* palmitoylation levels. However, the APEGS assay has a few points to note and limitations: 1) PEGs are easily degraded by oxygen in the air, 2) PEGs form complexes with SDS which have negative effects on SDS-PAGE and western blotting (Bermazzani *et al.*, 2004; Reichel, 2012), and 3) the present APEGS assay cannot be applied to proteomic analysis of *S*-palmitoylated proteins.

In addition to *S*-palmitoylation, the principle of the APEGS assay (*i.e.*, PEG-switch) was used for the quantification of *O*-glycosylation (Rexach *et al.*, 2010) and cysteine oxidation

(Makmura *et al.*, 2001; Burgoyne *et al.*, 2013). Given that cysteine residues are subjected to various post-translational modifications such as nitrosylation, sulfhydration, and so on (Couvertier *et al.*, 2014), I expect that the principle of the APEGS assay could be widely applied to these cysteine modifications. Very recently, while I prepared this thesis, a piece of related data was published reporting the PEG-switch assay to examine the palmitoylation states of phospholemman in ventricular myocytes (Howie *et al.*, 2014).

Depalmitoylation process of PSD-95

In 1987, Staufenbiel for the first time discovered the depalmitoylation process in erythrocytes (Stanfenbiel, 1987). Next year, he reported that the depalmitoylation reaction could be an enzymatic process (Stanfenbiel, 1988). On the other hands, it is possible that the depalmitoylation is a non-enzymatic event because the thioester bonds between cysteine thiols and palmitates are labile. In fact, Lypla1-mediated depalmitoylation of Hras and Gα in cells remains controversial, because these have been no definitive evidence showing their physiological roles. My experimental results indicate that the depalmitoylation of PSD-95 occurs with a half-life of about 2 hours (**Figure 9**) and was completely inhibited by treatment with Palm-B (**Figures 19B, 20B**). If Palm-B specifically acts on a subset of Lypla1-like serine hydrolases as originally proposed (Dekker *et al.*, 2010), it is speculated that the depalmitoylation of PSD-95 in neurons occurs by the enzymatic mechanism. However, the only way to definitively demonstrate this is to identify the authentic depalmitoylating enzyme,

whose loss of expression or functions completely blocks the depalmitoylation of PSD-95 in neurons.

Mathematical simulation indicates that the depalmitoylation at two cysteine residues of PSD-95 (Cys3 and Cys5) occurs at almost the same time ($k_1/k_2 = 0.1$) (**Figures 9C, 10F**). This result strongly suggests that the accessibility of the enzyme to tightly membrane-anchored PSD-95 is the rate-limiting step. Once the enzyme cleaves one of two thioester bonds, the rest of thioester bond is immediately cleaved. One may ask whether the second reaction is mediated by the same molecule sequentially or by the different kind of enzymes independently. Given that Lyplal forms the homodimers (Devedjiev *et al.*, 2000), the responsible enzyme may form oligomers for the immediate second reactions. Investigating the site specificity of the depalmitoylating enzyme may contribute to clarifying this issue.

ABHD17s are promising candidates for PSD-95 depalmitoylating enzymes

ABHD17 subfamily members are the most promising candidates for PSD-95 depalmitoylating enzymes as ABHD17B was partly localized in dendritic spines (**Figure 14**), interacted with PSD-95 (**Figure 17**), and robustly reduced the palmitoylation level of PSD-95 in neurons (**Figure 16**). In addition, ABHD17B was one of the targets of Palm-B that completely blocked the PSD-95 depalmitoylation in neurons (**Figure 19**). However, the triple knockdown of ABHD17 subfamily members in neurons did not show any effects on the

depalmitoylation process of PSD-95 (**Figure 20**), probably due to the incomplete knockdown of ABHD17s (80-90% reduction in mRNA levels but I could not evaluate the remaining protein levels), the molecular redundancy of P-PPTs or the existence of other authentic enzymes. Lypla1/2 may be other candidates for PSD-95 depalmitoylating enzymes as Lypla1/2 are original targets of Palm-B (Dekker *et al.*, 2010), are supposed to be localized at the membrane regions through its N-terminal palmitoylation (Kong *et al.*, 2013), and moderately reduced PSD-95 palmitoylation levels in HEK293T cells (**Figure 11**). However, Lypla1/2 double knockdown showed no effects on the depalmitoylation process of PSD-95 (**Figure 20**). Therefore, it is conceivable that both ABHD17s and Lypla1/2 cooperatively regulate PSD-95 depalmitoylation.

ABHD12/13 and ABHD17s are originated from an yeast ortholog, YNL320W. Recently, parasitic *Toxoplasma* protein TgPPT1 that shows a high homology to ABHD13 was reported as a depalmitoylating enzyme (Child *et al.*, 2013). However, ABHD13 (**Figure 14**) and its homologue ABHD12 (data not shown) were not localized at the post-synaptic or plasma membrane and did not show robust effects on the PSD-95 palmitoylation level in HEK293T cells (**Figure 11**). In addition, triple knockdown of ABHD12/13/16A did not affect the PSD-95 depalmitoylation process in neurons (**Figure 20**). Nevertheless, ABHD12/13 might compensate ABHD17s' functions in neurons. Therefore, it is worthwhile to examine the effects of multiple knockdown or knockout of these different P-PPT subfamilies.

Proposed reaction mechanism of ABHD17s

ABHD17B has a canonical α/β hydrolase fold and catalytic triad, Ser170, Asp235 and His264 (**Figure 15**). The catalysis of the canonical lipase, which has an α/β hydrolase fold, is composed of the following three steps: 1) acylation step, 2) formation of acyl-enzyme complex, and 3) nucleophilic attack by a water molecule (Cygler *et al.*, 1994; Grochulski *et al.*, 1994). Here, I constructed a reaction model of ABHD17-mediated depalmitoylating reaction (**Figure 21**). First, the hydroxyl group of Ser activated by Asp and His of the catalytic triad forms a tetrahedral ternary complex with a palmitoylated substrate (Step 1). Then, *O*-palmitoylated enzyme is formed, releasing a free-thiol cysteine of the substrate (Step 2). The subsequent nucleophilic attack of a water molecule to the *O*-acylated enzyme produces the tetrahedral *O*-palmitoylated enzyme intermediate (Step 3). Finally, the free palmitate is released (Step 4) and the enzyme returns to an initial form for the next reaction (Step 5). To demonstrate this reaction model, it is necessary to detect the *O*-palmitoylated ABHD17B form that is hydroxylamine-insensitive.

Proposed regulatory mechanism of ABHD17s

The model structure suggests that ABHD17B has a putative lid region over its catalytic triad (**Figure 15**). Several lipases have also the similar lid region to keep it inactive. When the lipases bind to membranes (*i.e.*, lipid-water interfaces), the lipases are generally activated

through the conformation change of the lid region to expose its catalytic triad, referred to as interfacial activation (Veger, 1997). Given that ABHD17B is recruited to the plasma membrane via its N-terminal palmitoylation (**Figure 18**), it is conceivable that the putative lid region of ABHD17s is uncovered when palmitoylated ABHD17s interact with the membrane. Further structural studies are required to prove the hypothesis.

The data that the enzymatic activity of ABHD17B is regulated by its own N-terminal palmitoylation (**Figure 18**) suggests the interdependent regulatory mechanism between DHHC PATs and ABHD17s. The increased palmitoylation levels of ABHD17s by DHHC PATs could increase their depalmitoylating activities. In turn, increased depalmitoylating activities of ABHD17s may reduce the autopalmitoylation levels of DHHC proteins, which is supposed to be essential for the DHHC PAT activity (Fukata *et al.*, 2004). Such a negative feedback loop between DHHC PATs and ABHD17s may keep the palmitoylation levels of substrate proteins at a certain level, contributing to the cellular homeostasis.

Conclusion

In my thesis, I developed a novel method that for the first time allows to quantitatively investigate the number of sites and the stoichiometry of *S*-palmitoylated proteins (**Chapter 1**). This method will provide a major breakthrough in the *S*-palmitoylation research field. In addition, I challenged to explore depalmitoylating enzymes that have not been discovered

since 1970s and I obtained promising candidates, the ABHD17 subfamily, as PSD-95 depalmitoylating enzymes (**Chapter 2**). ABHD proteins including ABHD17s may be not only responsible enzymes for PSD-95, but also for various types of *S*-palmitoylated proteins. Thus, my study will contribute to elucidating the molecular mechanism for reversible *S*-palmitoylation in diverse cellular contexts.

Figures and Figure legends

Contents

Figure 1	Principle of the APEGS assay	65
Figure 2	Selection of mPEGs	66
Figure 3	Validation of NEM blocking step	67
Figure 4	Titration of hydroxylamine treatment	68
Figure 5	Optimization of PEGylation condition	69
Figure 6	<i>S</i> -palmitoylation-dependent mobility shifts of PSD-95 and Hras	70
Figure 7	Verification of various neuronal palmitoyl proteins by the APEGS assay	71
Figure 8	Mathematical modeling of the PSD-95 palmitoylation cycle	72
Figure 9	Depalmitoylation processes of PSD-95 and Hras observed in the presence of 2-BP	73
Figure 10	Mathematical simulation of step-wise depalmitoylation processes	74
Figure 11	Screening for P-PPTs	75
Figure 12	Phylogenetic tree of mouse P-PPT candidates and ABHD family members	76
Figure 13	Gene expression of P-PPT candidates in cultured hippocampal neurons	77

Figure 14	Subcellular localization of P-PPT candidate proteins in neurons	78
Figure 15	Identification of catalytic triad of ABHD17 subfamily members	79
Figure 16	Ectopically expressed ABHD17B reduces the palmitoylation level of PSD-95 in neurons	80
Figure 17	Direct interaction of ABHD17B with PSD-95	81
Figure 18	Essential roles of N-terminal palmitoylation of ABHD17s in their localization and function	82
Figure 19	Screening of inhibitors for ABHD17B	84
Figure 20	Effects of P-PPT candidate knockdown on the PSD-95 depalmitoylation in neurons	85
Figure 21	A proposed depalmitoylating reaction of ABHD17s	86

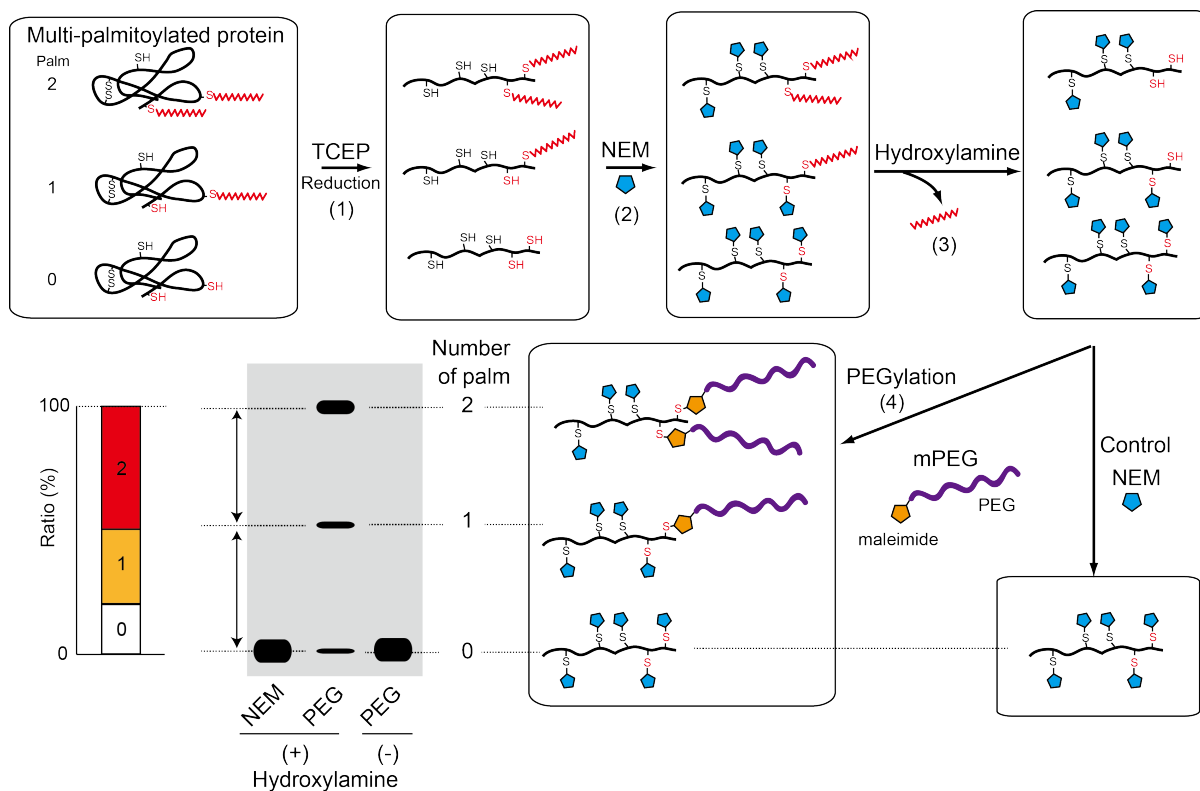


Figure 1. Principle of the APEGS assay

A protein with two palmitoyl cysteines is shown as a model protein. (1) Intra- and intermolecular disulfide bonds are reduced by TCEP. (2) Free cysteine residues are blocked with NEM. (3) Acyl-thioester linkages are cleaved by hydroxylamine. (4) mPEGs are incorporated into free thiol groups generated by the hydroxylamine treatment. Resultant samples are subjected to SDS-PAGE and western blotting with antibodies against proteins of interest. The NEM control lane indicates the original position of a target protein, corresponding to the position of non-palmitoylated protein. Hydroxylamine (-) lane indicates the negative control that is treated with tris instead of hydroxylamine at the step (3) to see the palmitoylation-dependent band shifts. Selective incorporation of PEG moieties with defined molecular weight could cause predictable shifts of protein bands, showing the number of palmitoylated sites of the protein. The ratio of individual palmitoylated forms, non-, mono-, and di-palmitoylated proteins is calculated by measuring the relative intensities of protein bands. S-S, disulfide bond; SH (black), free-cysteine thiol; SH (red), unoccupied/exposed palmitoyl cysteine thiol.

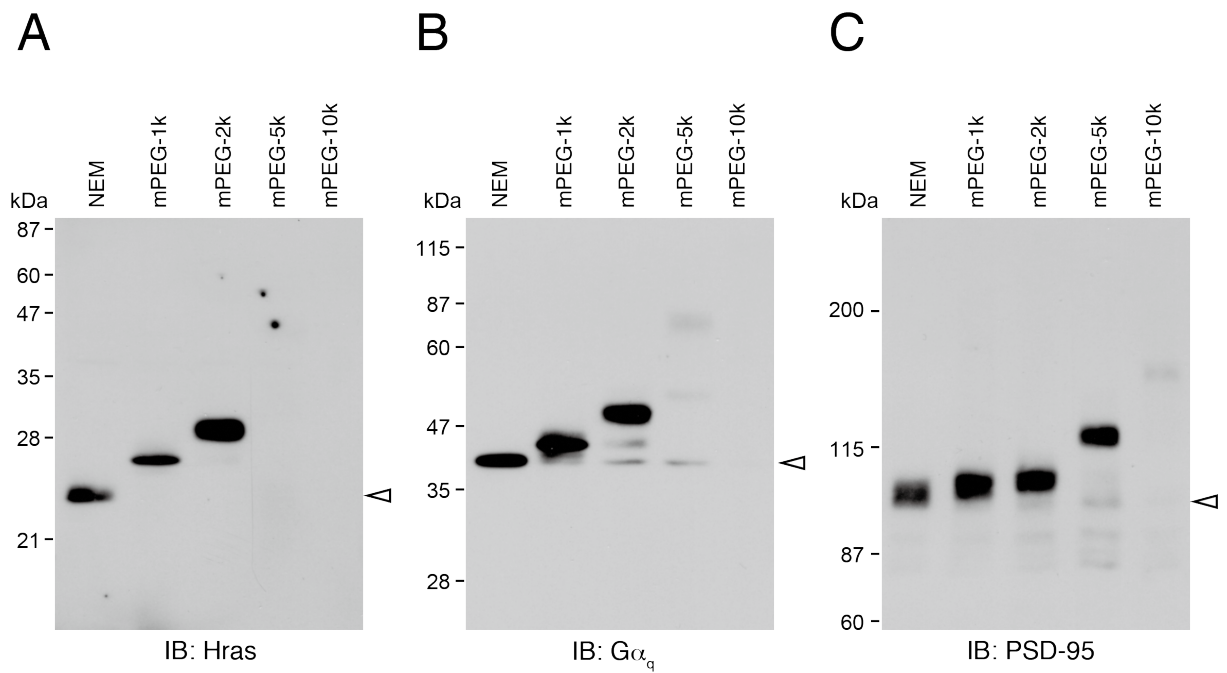
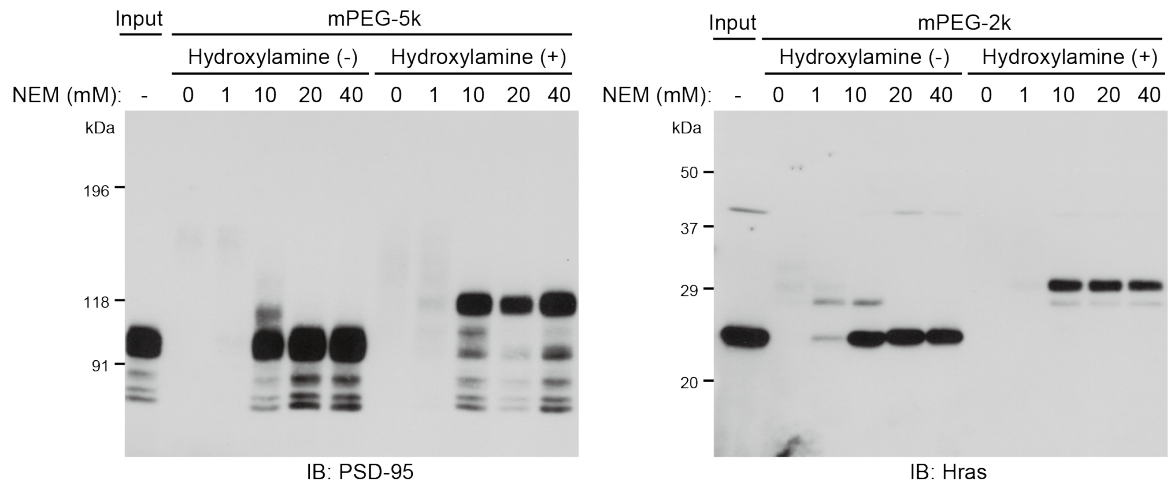


Figure 2. Selection of mPEGs

Cultured neuron lysates were sequentially treated with TCEP, NEM, and hydroxylamine. Then, samples were treated with 20 mM indicated mPEGs for 2 hours. Obtained samples were subjected to western blotting with Hras (A, ~21 kDa, 14% SDS-PAGE gel), G α_q (B, ~45 kDa, 10%) and PSD-95 (C, ~95 kDa, 6%) antibodies. Arrowheads represent the original position of target proteins.

A



B

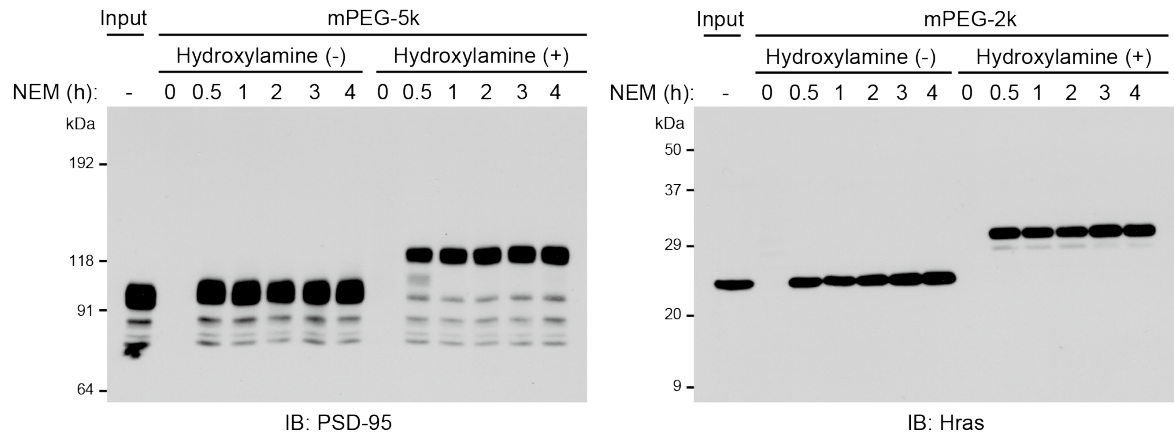
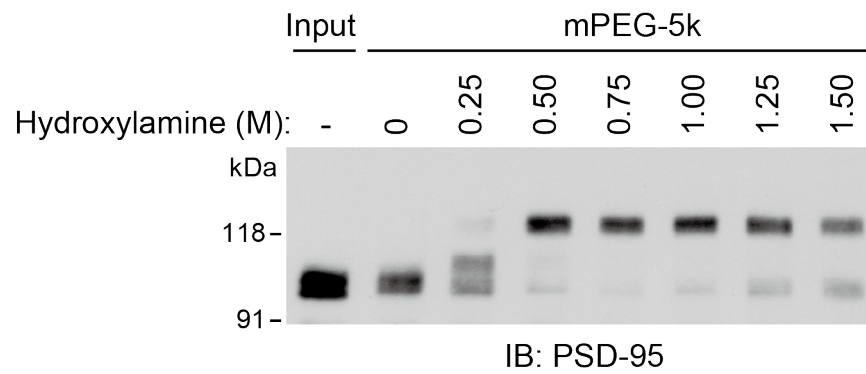
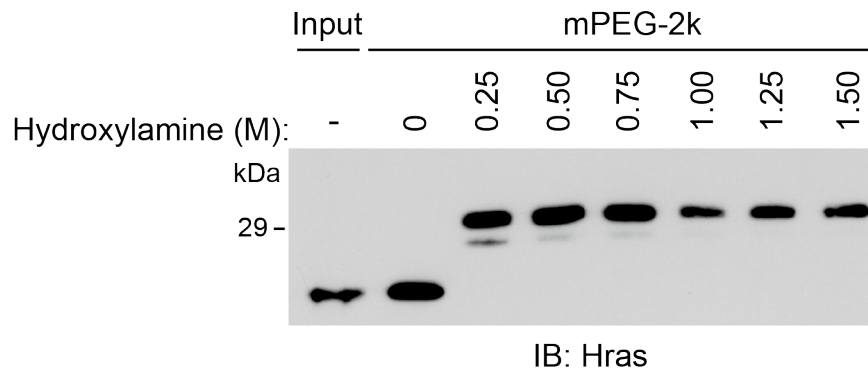


Figure 3. Validation of NEM blocking step

Doses (A) and incubation time (B) of NEM blocking in the APEGS assay. Cultured neuron lysates were treated with indicated concentrations of NEM for 3 hours (A) or treated with 40 mM NEM for the indicated time (B). Then, samples were treated with 1 M hydroxylamine and labeled with 20 mM mPEG.

A**B****Figure 4. Titration of hydroxylamine treatment**

Cultured neuron lysates were subjected to the APEGS assay. After blocking with NEM treatment (40 mM, 3 hour), lysates were treated with indicated concentrations of hydroxylamine for 1 hour at 37°C. Then, newly exposed free cysteine residues were labeled with 20 mM mPEG. Obtained samples were subjected to western blotting with PSD-95 (A) and Hras (B) antibodies.

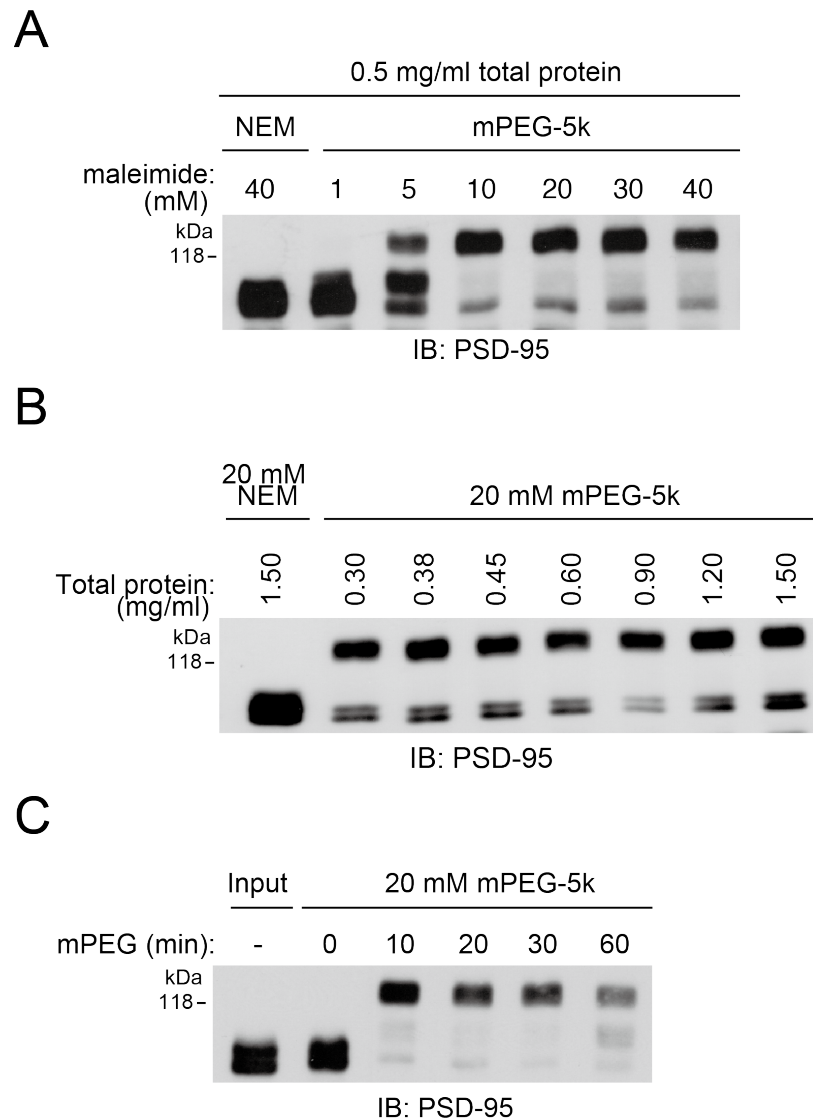


Figure 5. Optimization of PEGylation condition

Cultured neuron lysates were sequentially treated with NEM (40 mM, 3 hours) and hydroxylamine (1 M, 1 hour). (A) Doses of mPEG-5k for 0.5 mg/ml total proteins. (B) Doses of total proteins in the reaction for 20 mM mPEG-5k. (C) Incubation time with 20 mM mPEG-5k for 0.5 mg/ml total proteins. All samples were subjected to western blotting with PSD-95 antibody.

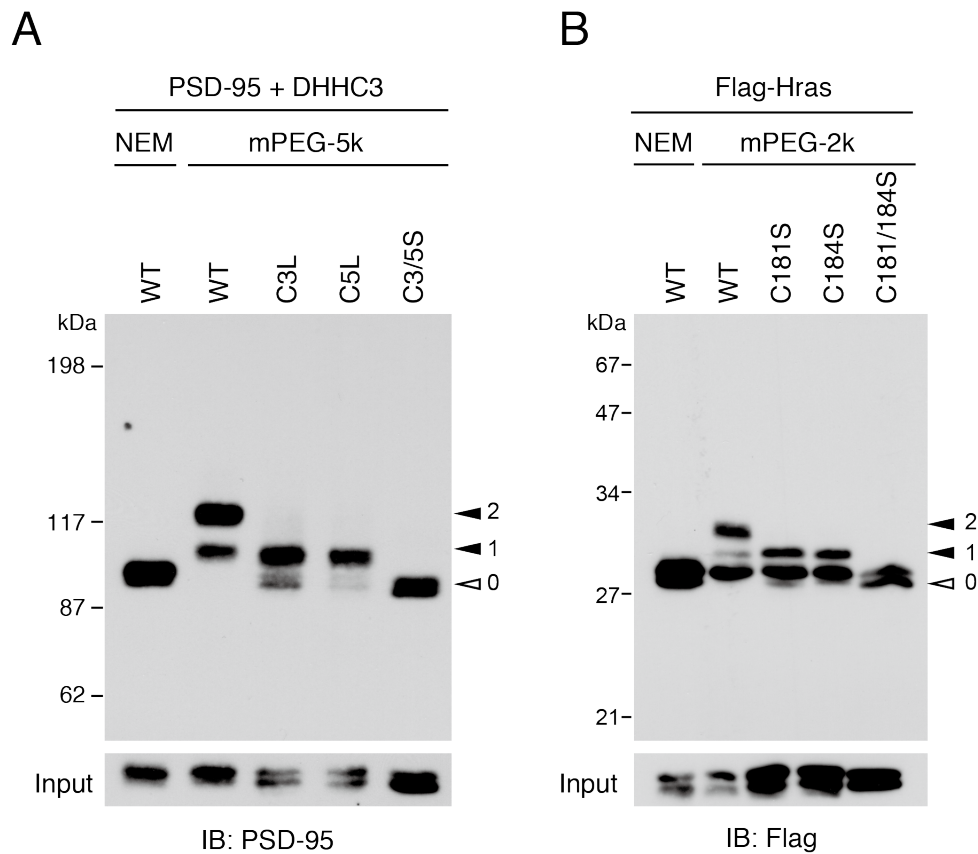


Figure 6. S-palmitoylation-dependent mobility shifts of PSD-95 and Hras

The APEGS assay for palmitoylation-deficient mutants of PSD-95 (A) and Hras (B). (A) PSD-95 WT and indicated mutants were co-expressed with DHHC3 in HEK293T cells. While PSD-95 WT had two slow-migrating bands in the presence of mPEG-5k, mono-palmitoyl C3L and C5L showed only one slow-migrating band without the slowest migrating band as detected for PSD-95 WT. Palmitoylation-deficient mutant C3/5S did not show any mobility shifts. (B) Flag-tagged Hras WT and indicated mutants were expressed in HEK293T cells. While Hras WT had two larger additional bands in the presence of mPEG-2k, mono-palmitoyl C181S and C184S showed only one additional band. Palmitoylation-deficient mutant C181/184S did not produce any slower-migration bands.

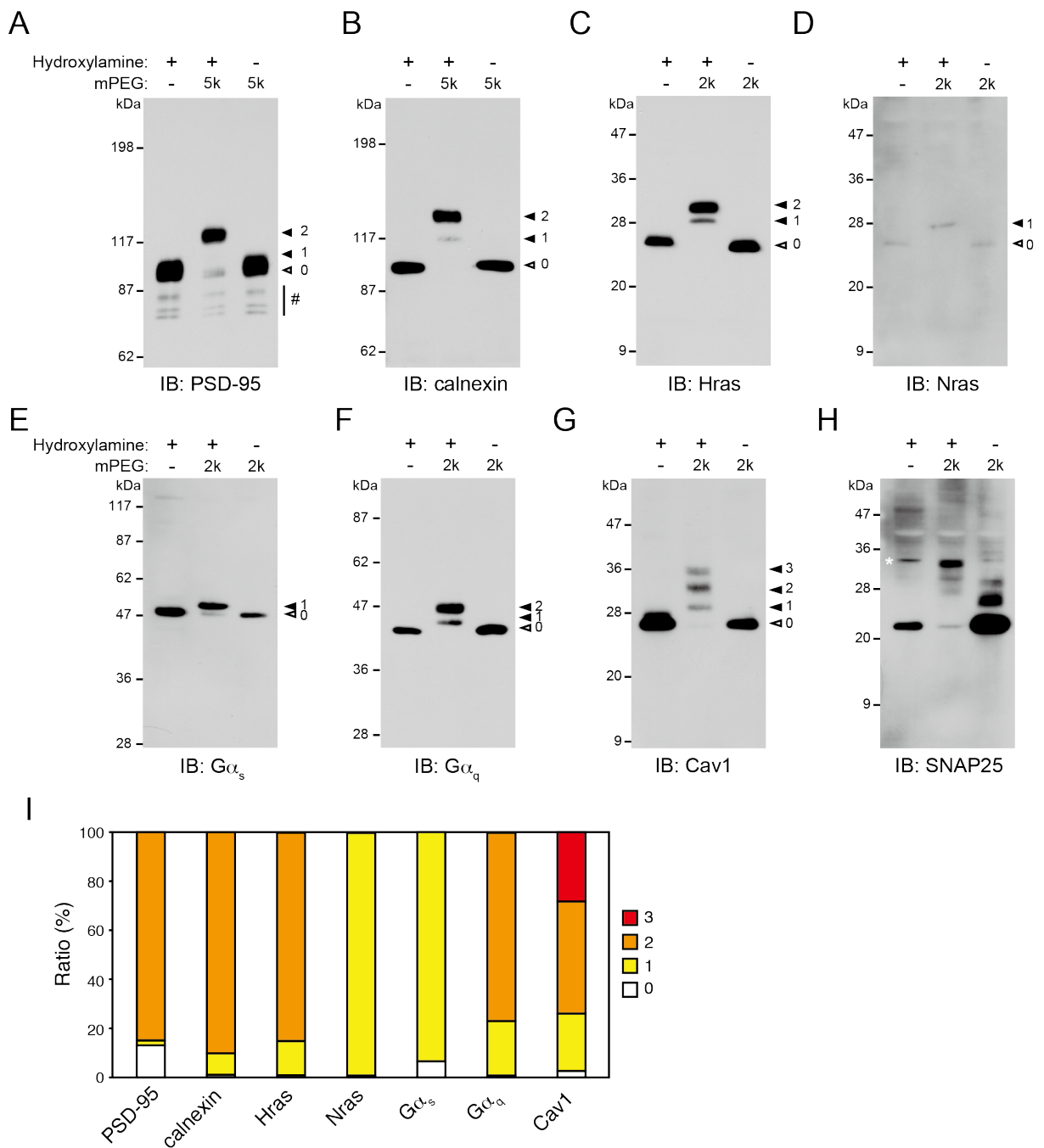


Figure 7. Verification of various neuronal palmitoyl proteins by the APEGS assay

Rat cultured hippocampal neurons were subjected to the APEGS assay and samples were analyzed by western blotting with the indicated antibodies. PSD-95 (A), calnexin (B), Hras (C), Nras (D), $G\alpha_s$ (E), $G\alpha_q$ (F), Cav1 (G) and SNAP25 (H). (I) The ratio of individual palmitoylation states (0, 1, 2, and 3) of proteins. # in (A) indicates bands of degraded PSD-95 proteins. * in (H) indicates a non-specific signal of anti-SNAP25 antibody.

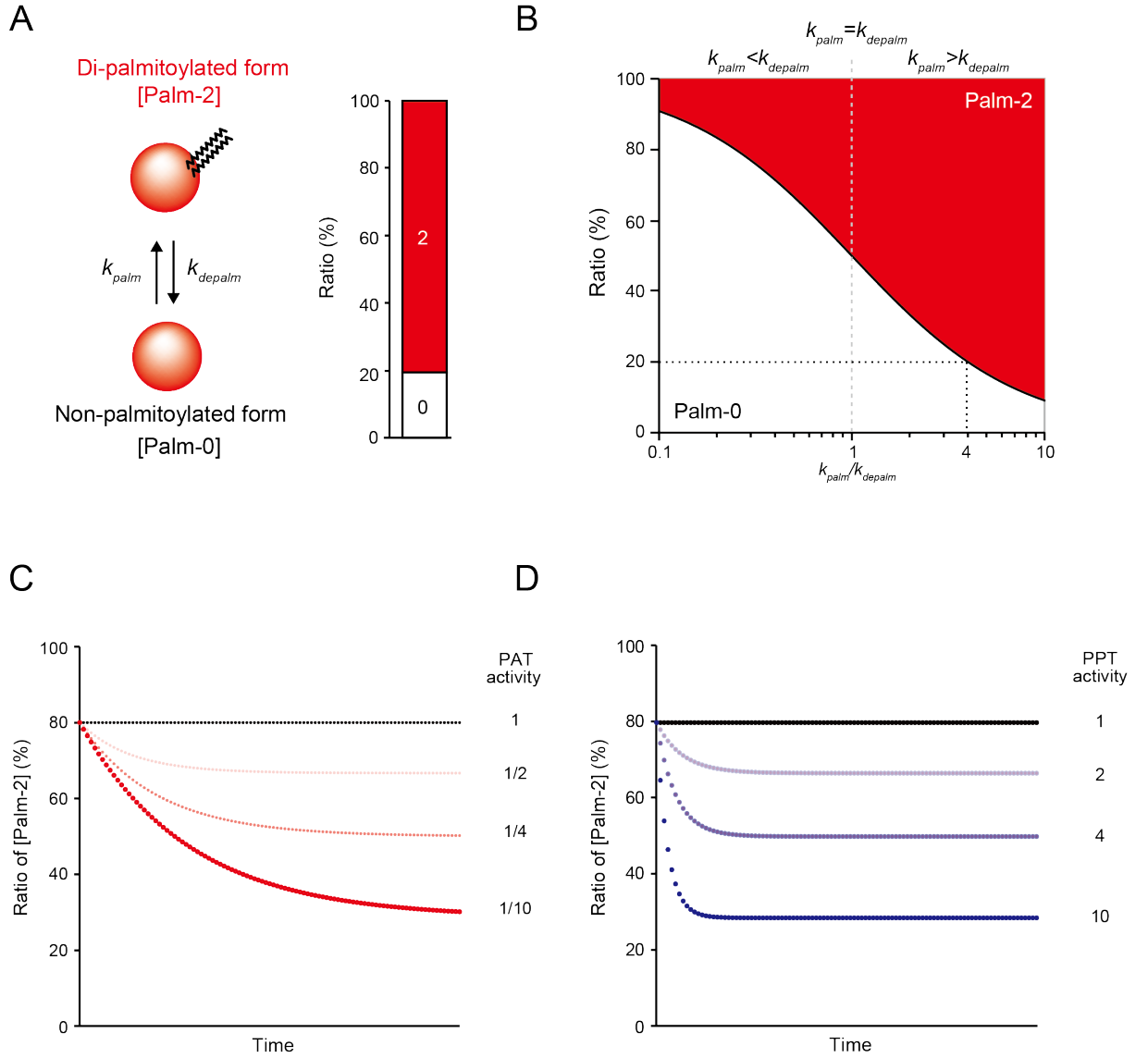


Figure 8. Mathematical modeling of the PSD-95 palmitoylation cycle

(A) A reversible first-order reaction model of the PSD-95 palmitoylation cycle. [Palm-2] and [Palm-0] represent amounts of di- and non-palmitoylated PSD-95. k_{palm} and k_{depalm} indicate rate constants of palmitoylation and depalmitoylation reaction, respectively. Based on Figure 7A and I, [Palm-2] and [Palm-0] are set at 80% and 20%, respectively. (B) The relationship between k_{palm}/k_{depalm} and ratio of two states calculated by Eq (4) in Materials and Methods. Red and white zones represent population of Palm-2 and Palm-0, respectively. When k_{palm}/k_{depalm} is 4, the ratio meets the initial setting ([Palm-2] and [Palm-0] are 80% and 20%, respectively). (C, D) Simulated responses of palmitoylation states of PSD-95 to perturbation of the palmitoylating enzyme (PAT) activity (C) and the depalmitoylating enzyme (PPT) activity (D).

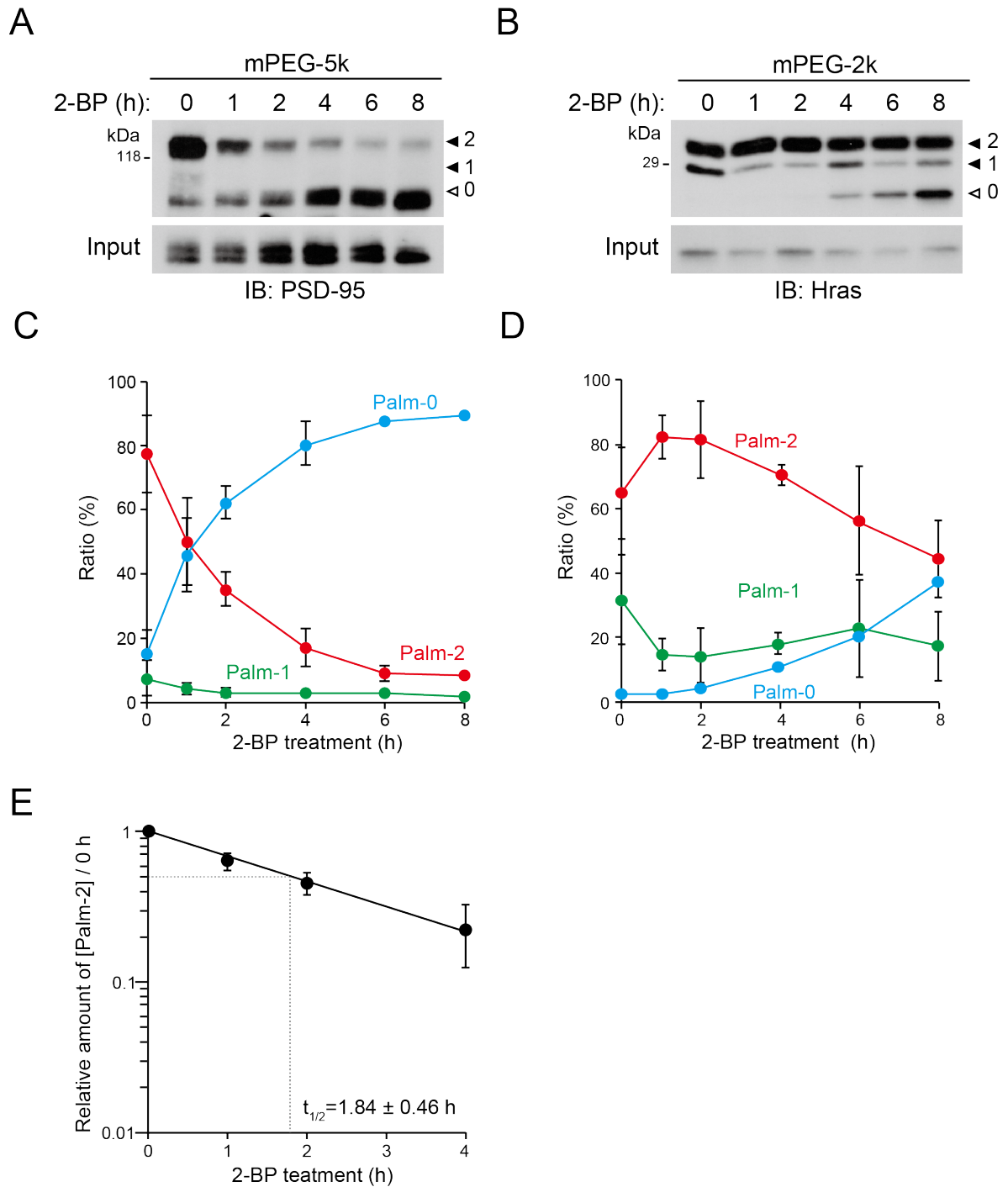


Figure 9. Depalmitoylation processes of PSD-95 and Hras observed in the presence of 2-BP

(A-D) The APEGS assay shows that treatment of rat hippocampal neurons with 100 μ M 2-BP reduces the amount of palmitoylated PSD-95 (A, C) and that of Hras (B, D). Values are mean \pm S.D. (n=3). (E) Decrease of the relative amount of di-palmitoylated PSD-95. The half-life was calculated to be 1.84 ± 0.46 hours. Values are mean \pm S.D. (n=3)

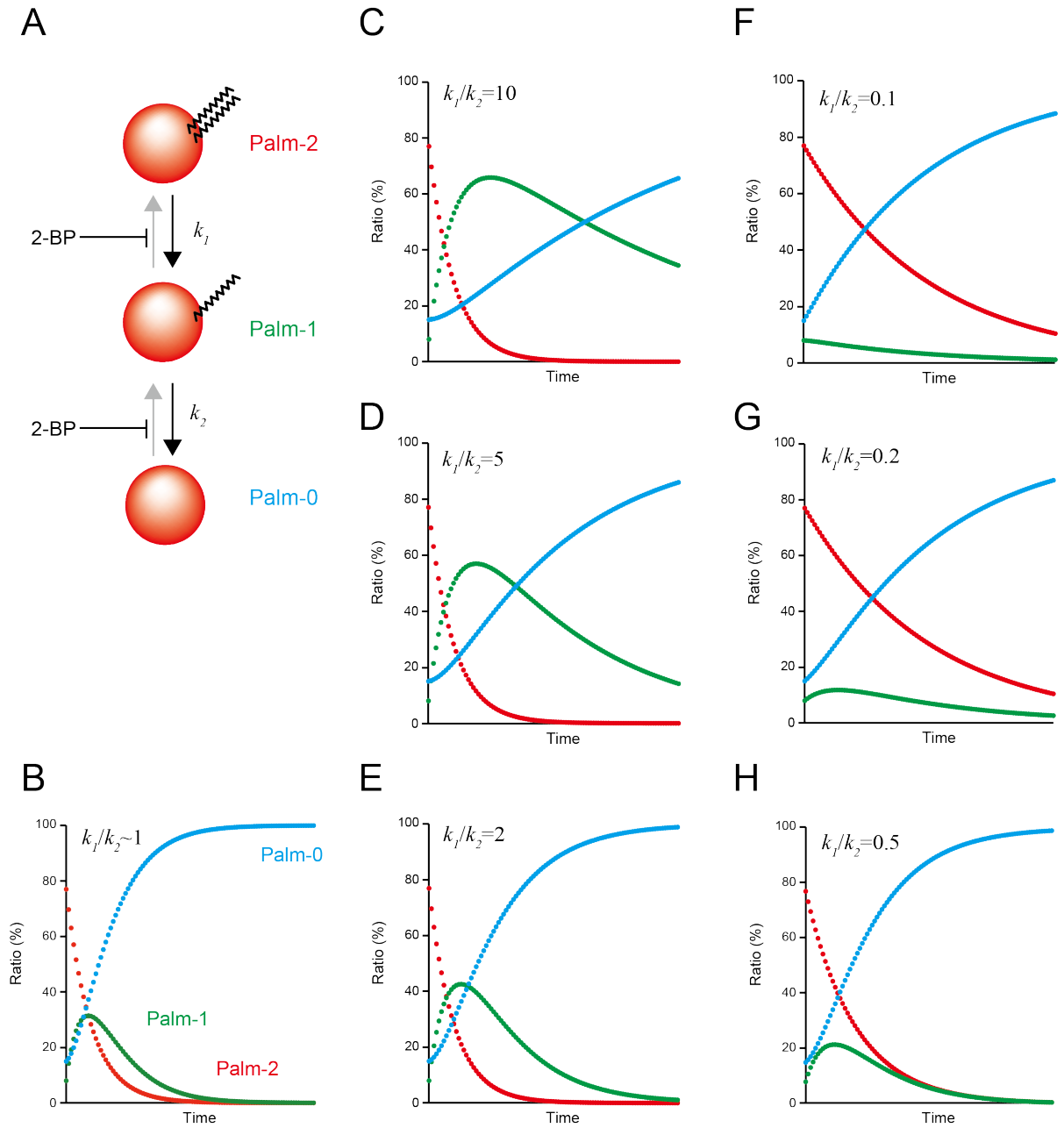


Figure 10. Mathematical simulation of step-wise depalmitoylation processes

(A) The 2-step depalmitoylation model in the presence of 2-BP. (B-H) PSD-95 depalmitoylation process was simulated by assuming various k_1/k_2 values. $k_1/k_2 \sim 1$ (B), $k_1/k_2 = 10$ (C), $k_1/k_2 = 5$ (D), $k_1/k_2 = 2$ (E), $k_1/k_2 = 0.1$ (F), $k_1/k_2 = 0.2$ (G), and $k_1/k_2 = 0.5$ (H). $k_1/k_2 = 0.1$ (F) is well consistent with the experimental depalmitoylating process of PSD-95 (Figure 9C).

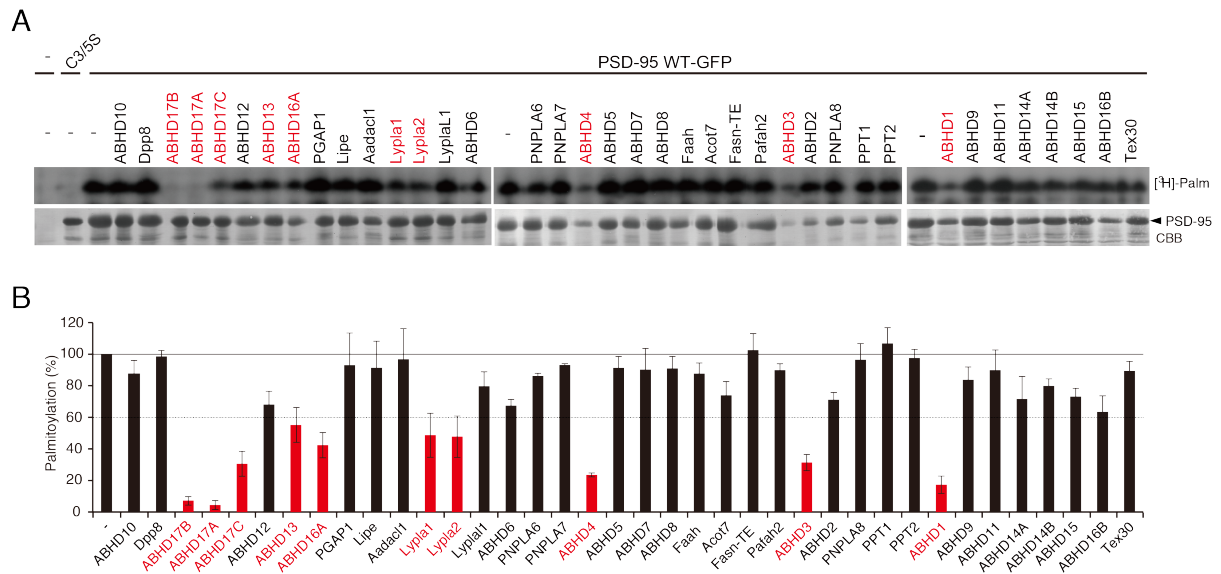


Figure 11. Screening for P-PPTs

(A) I isolated 38 uncharacterized serine hydrolase genes containing classical Lypla1/2, Lypla11, PPT1/2, HDEP-sensitive hydrolases, and ABHD proteins. Individual clones were co-transfected with PSD-95-GFP (WT or C3/5S, a palmitoylation-deficient mutant of PSD-95 in which Cys3 and Cys5 were replaced with Ser) into HEK293T cells. After metabolic labeling with [3 H]-palmitate, proteins were separated by SDS-PAGE, followed by fluorography (upper panel) and coomassie brilliant blue (CBB) staining (lower panel). (B) Quantitative analysis was performed by Image J. I selected 10 clones (indicated in red) that reduced PSD-95 palmitoylation levels to less than 60% compared with control of the basal level (the most left bar). Values are mean \pm S.D. (n=3)

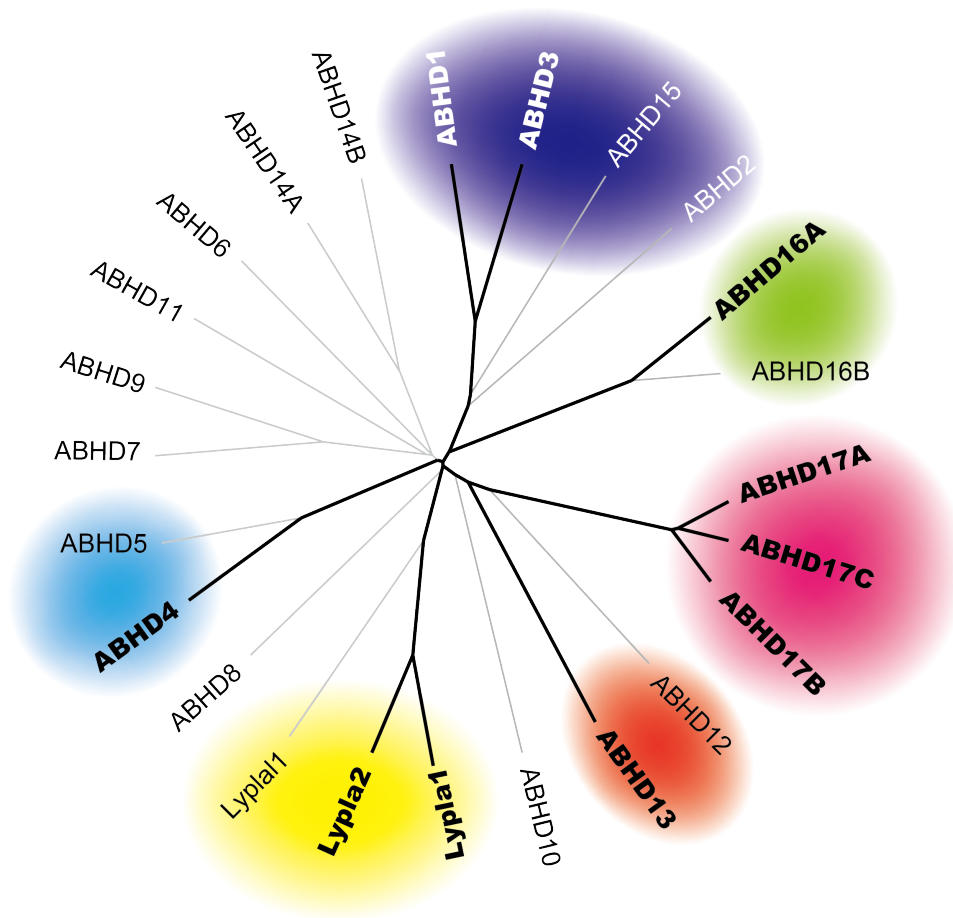


Figure 12. Phylogenetic tree of mouse P-PPT candidates and ABHD family members

Primary sequence alignments were performed by Clustal W2 and the phylogenetic tree was generated by Sea View. I used α/β hydrolase fold sequences of individual proteins for the alignment (Table 5). Bold proteins showed depalmitoylating activities toward PSD-95. Putative subgroups were classified by different color ovals.

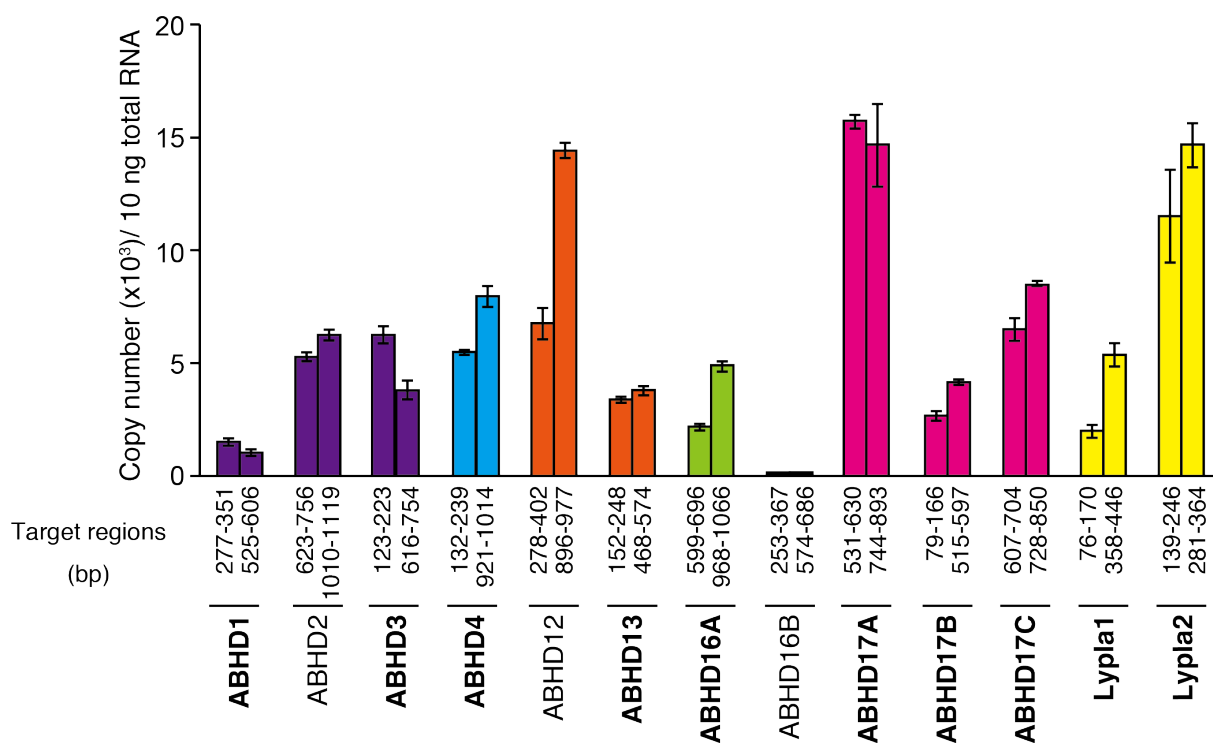


Figure 13. Gene expression of P-PPT candidates in cultured hippocampal neurons

Total RNA was extracted from cultured rat hippocampal neurons and cDNA was synthesized by High-Capacity cDNA RT kit. The copy numbers of target cDNAs in 10 ng of total RNA were quantified by the absolute quantification of real-time PCR. Assays were performed by two independent primer pairs (Table 3). Bold proteins showed depalmitoylating activities toward PSD-95. Putative subgroups were classified by different color. Values are mean \pm S.D. (n=3)

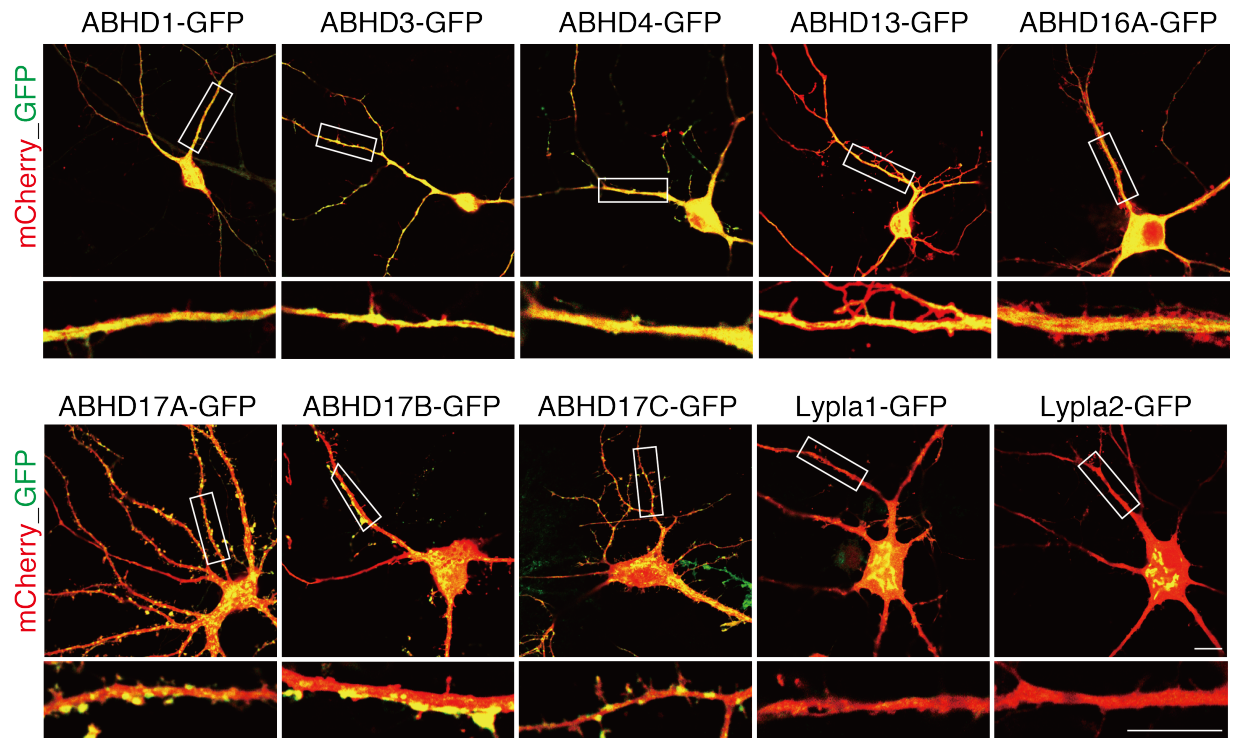


Figure 14. Subcellular localization of P-PPT candidate proteins in neurons

Indicated GFP-tagged P-PPT proteins were transfected with mCherry as a volume marker into rat hippocampal neurons (20-22 DIV). Only ABHD17 subfamily members were localized in dendritic vesicles and spines. ABHD1, 3, 13, and 16A were localized in endomembranes. ABHD4 was diffusely localized in the cytoplasm. Lypla1/2 strongly accumulated at the Golgi apparatus as well as in the cytoplasm. Bars: 10 μ m.

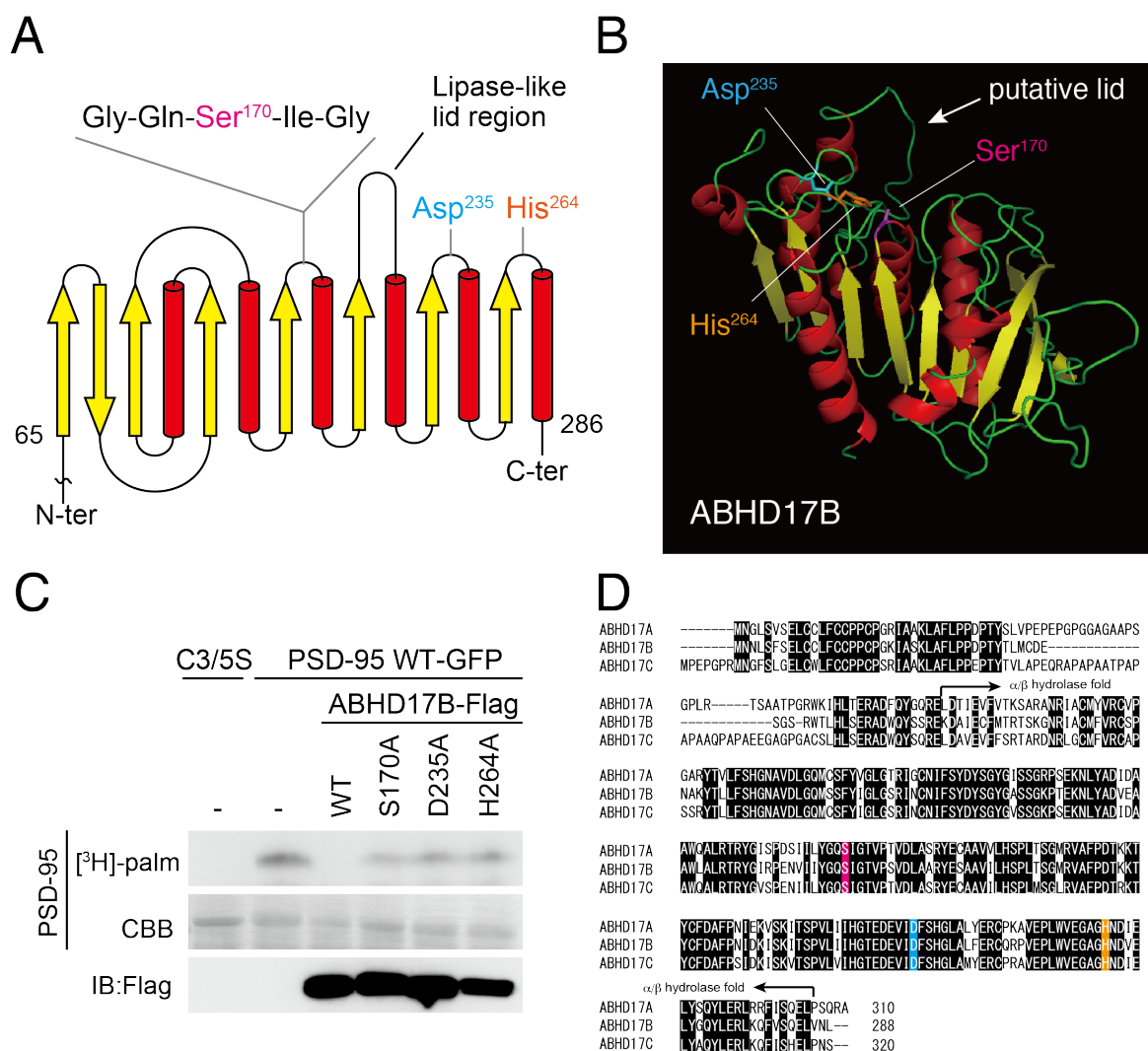


Figure 15. Identification of catalytic triad of ABHD17 subfamily members

(A) A secondary structure of an α/β hydrolase fold (amino acid, 65-286) of ABHD17B, which contains 6 α -helices (red columns) and 8 β -sheets (yellow arrows). A catalytic serine residue, Ser170, was predicted in the conserved motif Gly-Xaa-Ser-Xaa-Gly (Xaa: any amino acids). (B) The predicted structure of full-length ABHD17B by an *in silico* homology-modeling software, HH-pred. The modeling revealed that Asp235 and His264 are close to Ser170 at loops between α -helices and β -sheets. ABHD17B has a lipase-like putative lid region (white arrow) that usually regulates lipids interactions and enzymatic functions of lipases. (C) Predicted catalytic triad amino acids are essential for the activity of ABHD17B. The indicated ABHD17B mutants were subjected to metabolic [³H]-palmitate labeling assay as in Figure 11. No mutants showed reductions of [³H]-palmitate signals of PSD-95. (D) Sequence alignment of mouse ABHD17 subfamily members. All catalytic amino acids are conserved among subfamily members.

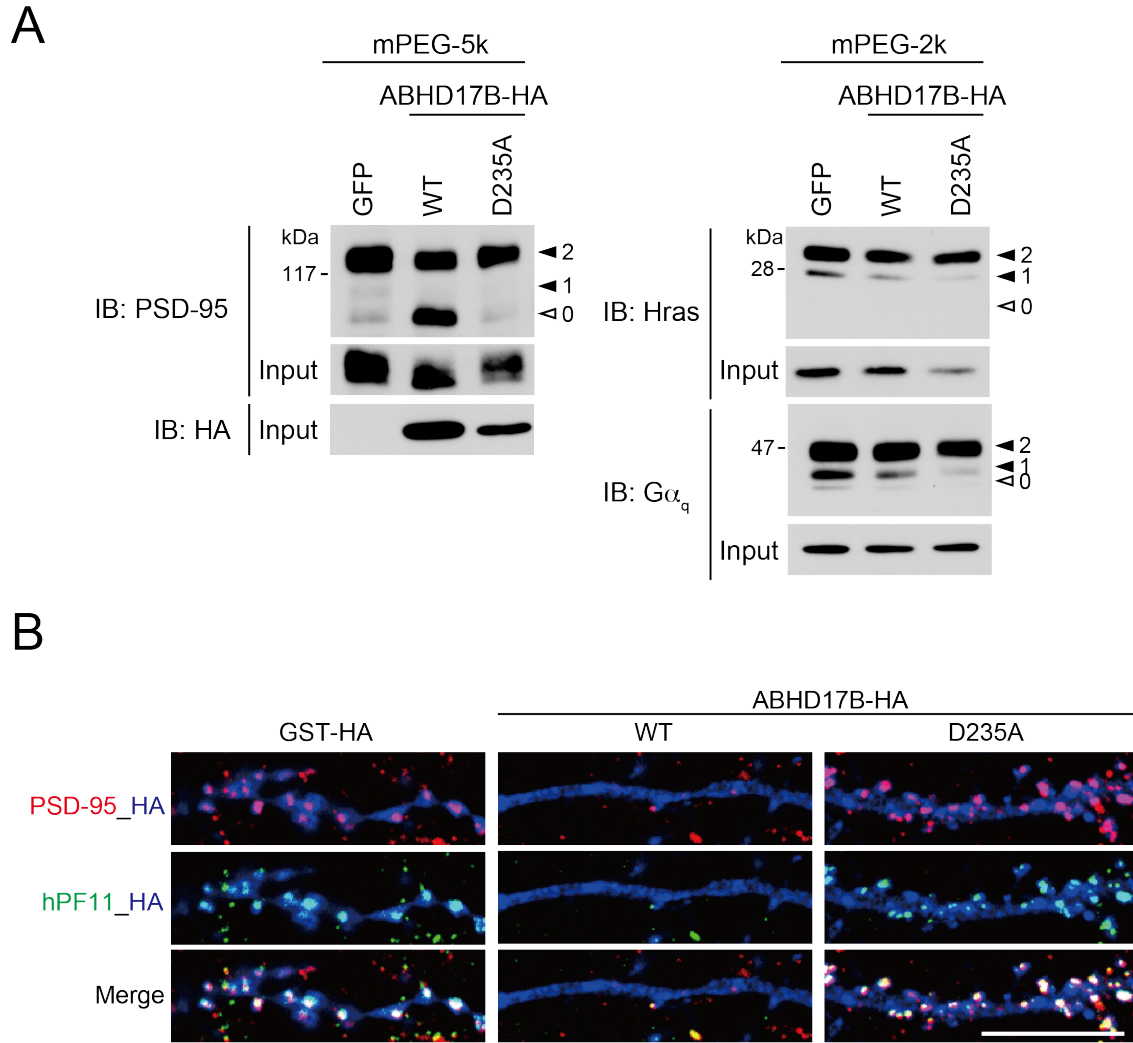
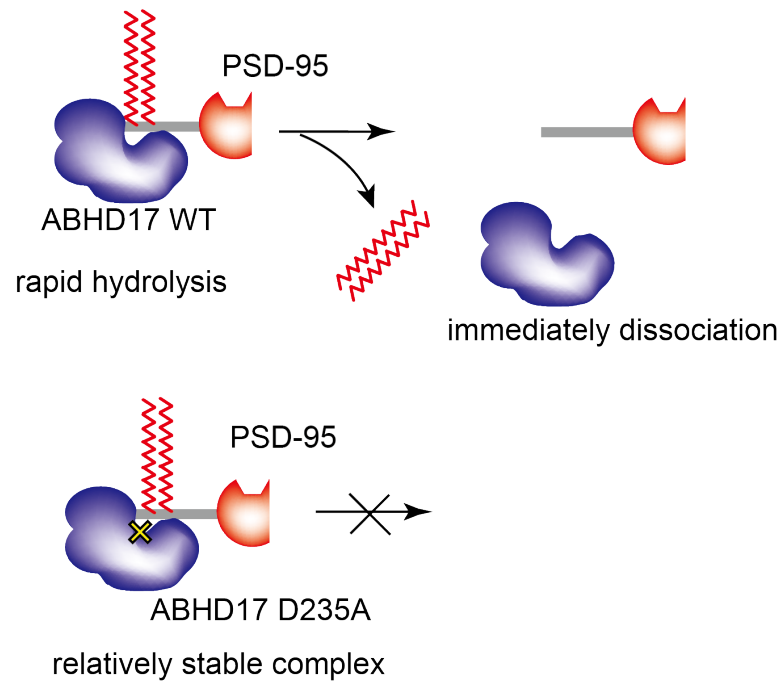


Figure 16. Ectopically expressed ABHD17B reduces the palmitoylation level of PSD-95 in neurons

ABHD17B-HA WT or D235A was overexpressed in rat hippocampal neurons by AAV-DJ vectors (A) or lipofection (B). (A) GFP-, ABHD17B-HA WT- or D235A-overexpressing neurons were subjected to the APEGS assay. GFP was used for a negative control. The palmitoylation level of endogenous PSD-95 was specifically reduced in ABHD17B WT-, but not ABHD17B D235A-expressing neurons. In contrast, ABHD17B WT did not affect palmitoylation levels of Hras and $G\alpha_q$. One representative result from three independent experiments is shown. (B) ABHD17B-HA WT-, D235A-, or GST-HA (negative control)-overexpressing neurons were stained by anti-HA antibody (blue), anti-PSD-95 antibody (red) and palmitoylated PSD-95 specific probe, hPF11 (green). ABHD17B-HA WT, but not D235A, dramatically reduced both clusters of total and palmitoylated PSD-95. Bar: 10 μ m.

A



B

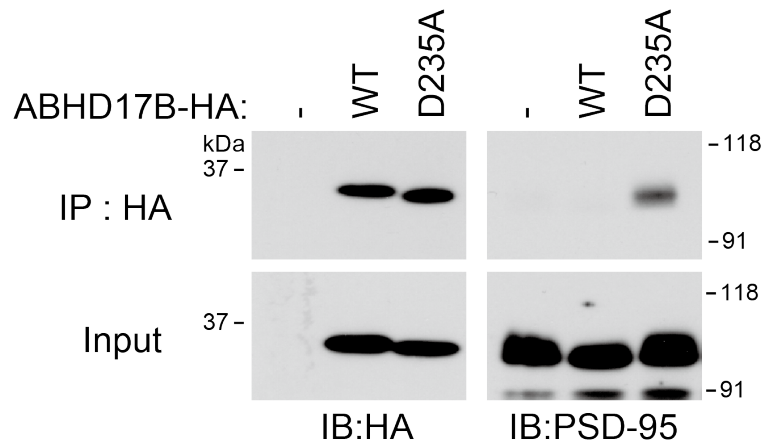


Figure 17. Direct interaction of ABHD17B with PSD-95

(A) Scheme of the binding assay using a catalytically inactive ABHD17B D235A mutant as a substrate-trapping mutant. Generally, it is difficult to detect the transient interaction between a hydrolase and its substrate via its catalytic region. On the other hand, the catalytic inactive mutant could form relatively stable complex with the substrate. (B) Ectopically expressed ABHD17B-HA WT or D235A by AAV-DJ was immunoprecipitated with anti-HA antibody from hippocampal neurons. Then, co-precipitated PSD-95 was detected in only ABHD17B D235A-expressed neurons. One representative result from three independent experiments is shown.

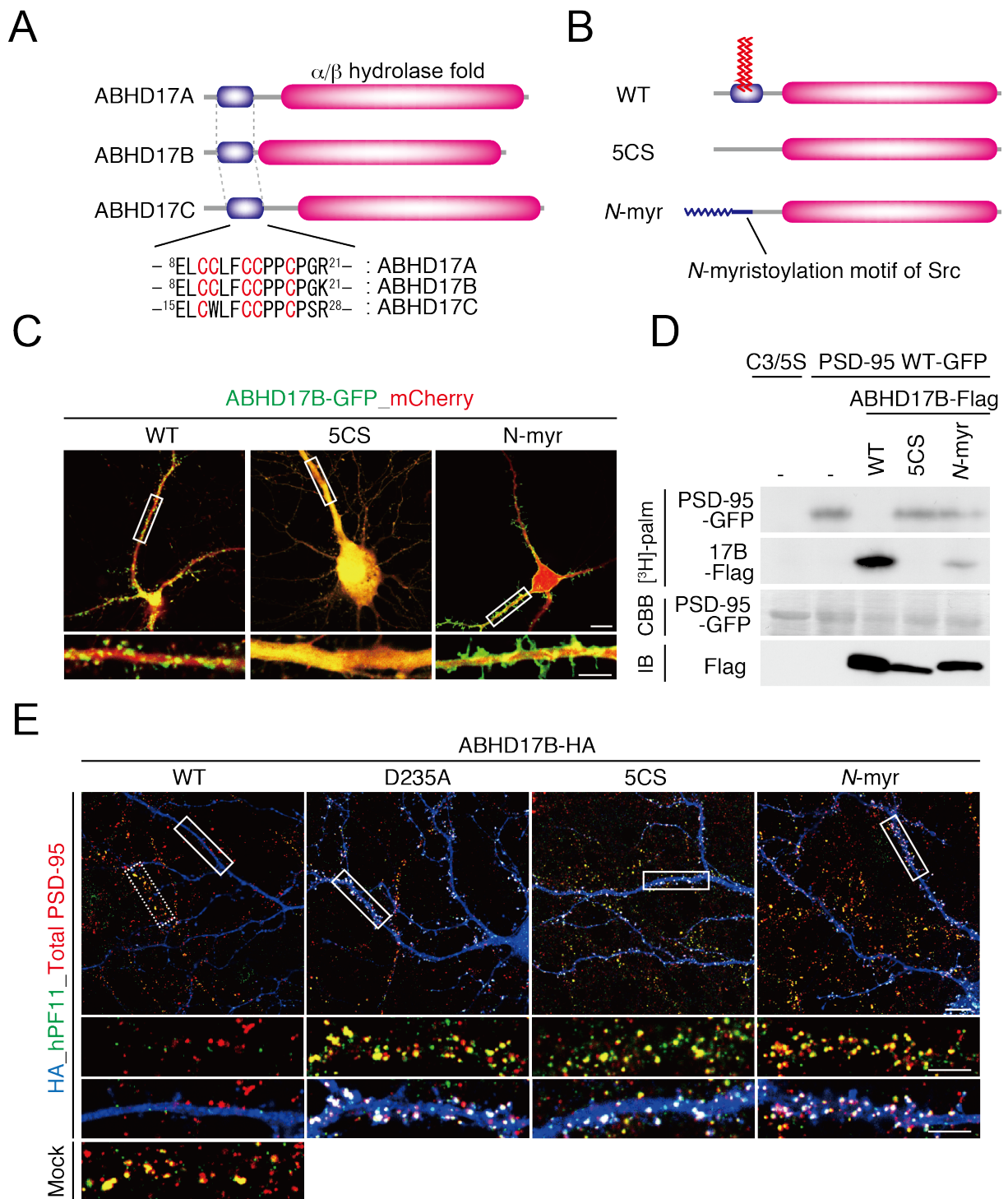
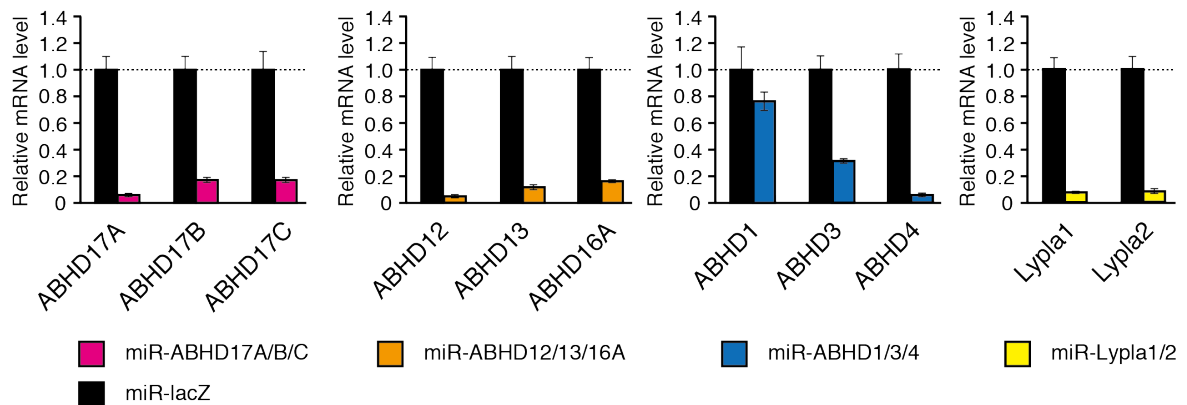


Figure 18. Essential roles of N-terminal palmitoylation of ABHD17s in their localization and function

(A) Structures of ABHD17 members. ABHD17s have palmitoylated cysteine clusters at N-terminal regions. (B) Structures of ABHD17B chimeric constructs: the palmitoylated WT, a palmitoylation-deficient 5CS (C10/11/14/15/18S), and an irreversibly N-myristoylated N-myr [Src(1-20)/ABHD17B(21-288)]. (C) Subcellular localization of ABHD17B mutants (green). WT was specifically localized in dendritic vesicles and spines. In contrast, 5CS was

diffusely localized in the cytoplasm and *N*-myr was localized at the plasma membrane. mCherry was used as a volume marker (red). Bars: 10 μm (upper panel) and 5 μm (lower panel). (D) Enzymatic activities of ABHD17B mutants tested by the metabolic labeling assay as in Figure 11. Both mutants lost their depalmitoylation activity for PSD-95 ($[^3\text{H}]$ -palm, upper panel). ABHD17B WT was highly palmitoylated, but 5CS was not ($[^3\text{H}]$ -palm, lower panel). Weak labeling of *N*-myr ABHD17B might be due to *N*-palmitoylation. (E) Effects of ectopically expressed HA-tagged ABHD17B mutants (blue) on post-synaptic clusters of endogenous PSD-95. ABHD17B WT dramatically reduced clusters of total (red) and palmitoylated PSD-95 (green), but mutants did not affect. Bars: 10 μm (upper panel) and 5 μm (lower panel).

A



B

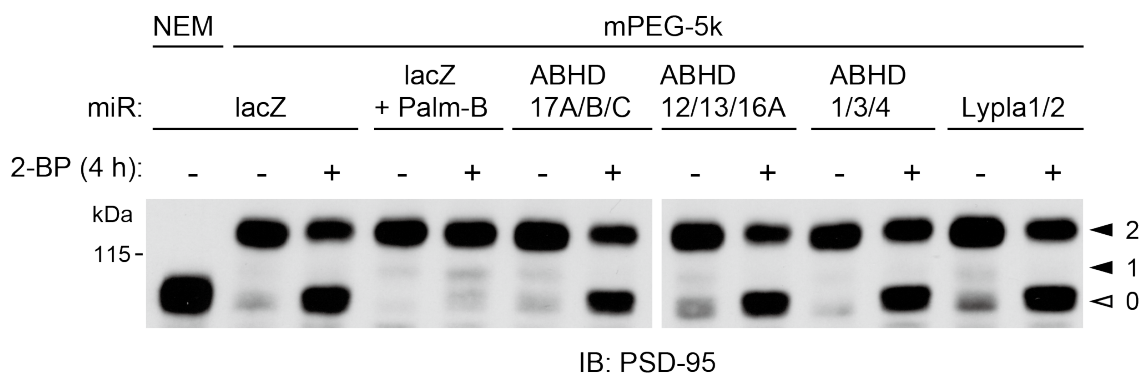


Figure 20. Effects of P-PPT candidate knockdown on the PSD-95 depalmitoylation in neurons

Rat hippocampal neurons (13 DIV) were multiply infected with AAV-DJ:EmGFP-miRNAs for ABHD17A/B/C (magenta), ABHD12/13/16A (orange), ABHD1/3/4 (blue), and Lypla1/2 (yellow) (Table 2). miR-lacZ (black) was a negative control. After 6 days infection, relative mRNA expression levels were estimated by real-time PCR (A). Values are mean \pm S.D. (n=3). After 7 days infection, infected neurons were treated with 2-BP (100 μ M) in the presence or absence of Palm-B (100 μ M) for 4 hours and subjected to the APEGS assay (B). Treatment with Palm-B, as a positive control, clearly inhibited the depalmitoylation process of PSD-95. However, under the experimental conditions, I could not see any knockdown effects on the PSD-95 depalmitoylation.

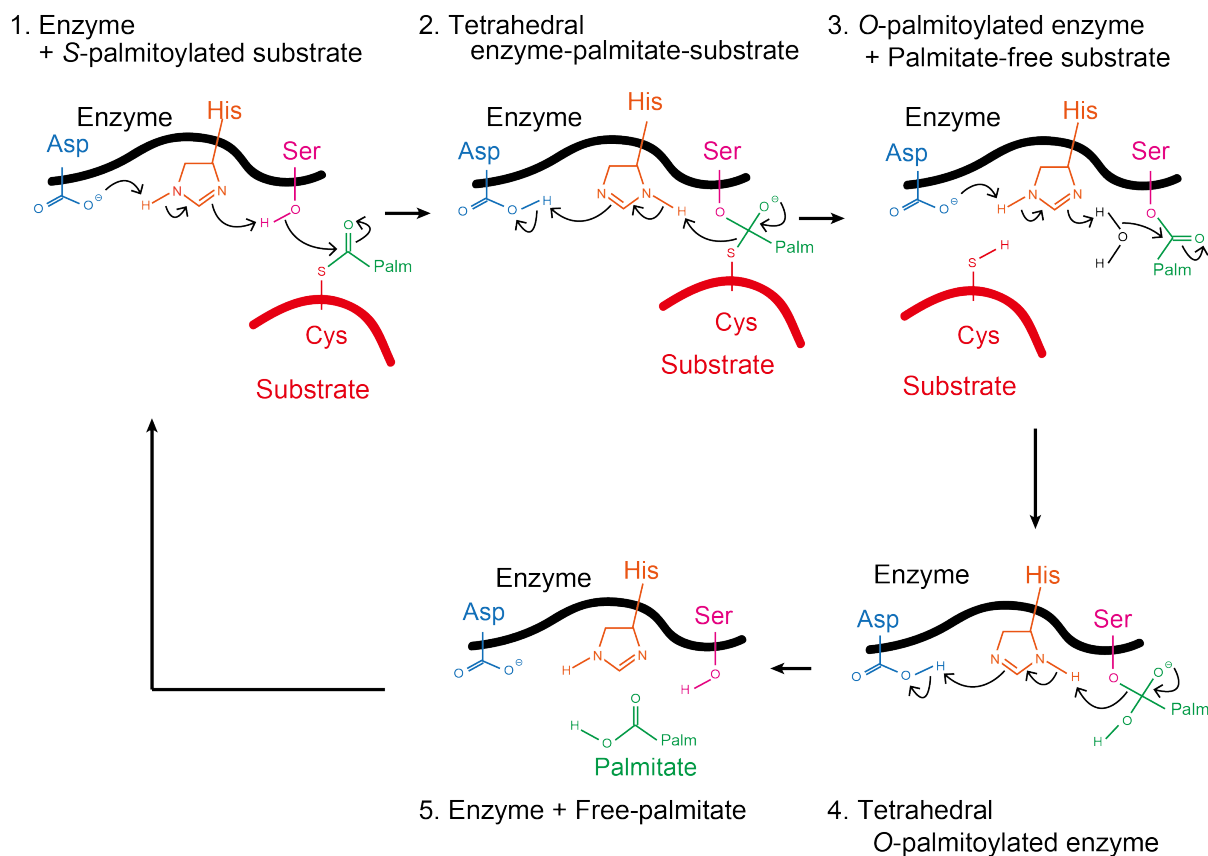


Figure 21. A proposed depalmitoylating reaction of ABHD17s

Step 1) The catalytic serine residue is activated by Asp and His and attacks to the thioester moiety of the *S*-palmitoylated protein. Step 2) The tetrahedral ternary complex is formed and a substrate protein is released as an elimination group. Step 3) A water molecule attacks to the *O*-acylated enzyme. Step 4) The tetrahedral *O*-palmitoylated enzyme is transiently formed and the free palmitate is released as an elimination group. Step 5) The enzyme returns to an initial form.

Tables

Contents

Table 1	List of isolated genes as candidates for depalmitoylating enzymes	88
Table 2	miRNA target sequences and top/bottom oligo DNAs	89
Table 3	List of primer pairs for real-time PCR	90
Table 4	Calculated molecular weights of PEGylated proteins	91
Table 5	α/β hydrolase fold regions of mouse ABHD and Lypla proteins used to construct the phylogenetic tree	92
Table 6	Contrasting characteristics of the APEGS assay and previous methods for <i>S</i> -palmitoylation analysis	93

Table 1 List of isolated genes as candidates for depalmitoylating enzymes

Official symbol	Gene name	Species	Accession No.	Forward primer	Reverse primer
ABHD1	abhydrolase domain containing 1	Rattus noviegicus	NM_001008520	5'-GCTAGAATTACACCATGGAATACCTCCACATAACCAAGAT-3'	5'-GCTAAGATCTGCTCTTCCATCTTCCAGGAGTGAAT-3'
ABHD2	abhydrolase domain containing 2	Rattus noviegicus	NM_001106275	5'-GCTAGAATTACACCATGGAATACCTCCATGTTGGAGACCCC-3'	5'-GCTAGAATCTTCTTAATCTCGCCTCCATCTGCT-3'
ABHD3	abhydrolase domain containing 3	Rattus noviegicus	NM_001106162	5'-GCTATTAAATTAACCATGCGAGCGCTGGCCGATGATCT-3'	5'-GCTAGGTACCATGTTGGAGATCTCATCTGCATGC-3'
ABHD4	abhydrolase domain containing 4	Rattus noviegicus	NM_001108866	5'-GCTATTAAATTAACCATGGGCTGGCTCAGCTGCACCC-3'	5'-GCTAGGTACCATGTTGGAGATCTCATCTGCATGC-3'
ABHD9	abhydrolase domain containing 9	Rattus noviegicus	NM_001108988	5'-GCTAGAATTACACCATGCGGCTGGCTGCTCTTATCC-3'	5'-GCTAAGATCTGCCACGAGGCTTGTGCAAGAAG-3'
ABHD12	abhydrolase domain containing 12	Rattus noviegicus	NM_001024314	5'-GCTAGGTACCATGATGAGGAGCGAGCCGCT-3'	5'-GCTAGGTACCATGCTGGCGCTCTGTTCCGACT-3'
ABHD13	abhydrolase domain containing 13	Rattus noviegicus	NM_001271072	5'-GCTAGGTACCATGATGAGGAGCCCTGGATGCTGTG-3'	5'-GCTAGGTACCATGATGAGGAGCCATGATGATGATG-3'
ABHD14A	abhydrolase domain containing 14A	Rattus noviegicus	NM_001009670	5'-GCTAGAATTACCATGAGCGCTACAGGCGACCC-3'	5'-GCTAAGATCTAGGCAATGGTCAAGAAAGCAAGG-3'
ABHD14B	abhydrolase domain containing 14B	Rattus noviegicus	NM_001007664	5'-GCTAGAATTACCATGCGCAATGGAGCTGAGTGA-3'	5'-GCTAGAATTCAGCTAGCTCTCTGCGAGGAGTCC-3'
ABHD15	abhydrolase domain containing 15	Rattus noviegicus	NM_001107025	5'-GCTATTAAATTAACCATGCTCGTGGCGAGCCGCC-3'	5'-GCTAGGTACCATGCTGTAAGAACCTTCCAGTC-3'
ABHD16A	abhydrolase domain containing 16A	Rattus noviegicus	NM_212531	5'-GCTAGAATTACCATGCGGAAGCTGCTGAGCTGCGT-3'	5'-GCTAGAATTCGAGCACGAGGCAATCGGAAGT-3'
ABHD16B	abhydrolase domain containing 16B	Rattus noviegicus	NM_001014052	5'-GCTAGAATTACCATGCGGCTGCTGCTGTTGAAAGG-3'	5'-GCTAGAATTCAGTCTCCAGGCAATTTGGAAGTCT-3'
ABHD17A	abhydrolase domain containing 17A	Rattus noviegicus	NM_145421	5'-GCTAGAATTACCATGAGCGCTGTCGGTAGCGGA-3'	5'-GCTAGAATTCGGTGGCTGGGAGCTCT-3'
ABHD17B	abhydrolase domain containing 17B	Rattus noviegicus	NM_001014028	5'-GCTAGAATTACCATGAATATCTTCAATTAGTGAGCT-3'	5'-GCTAGAATTCAGATTCACAGTCTCTGTGACACAA-3'
ABHD17C	abhydrolase domain containing 17C	Rattus noviegicus	NM_001100736	5'-GCTAGAATTACCATGCGCGAGCCGCCGAGGAT-3'	5'-GCTAGAATTCGGAGGAGCTCGTGAGATA-3'
Tex30	testis expressed 30	Rattus noviegicus	NM_001106909	5'-GCTAGAATTACCATGAGTCAACAGAGTTAAATAAAT-3'	5'-GCTAGAATTCATACATTTCTTGTCATTCAGTGATT-3'
Lypla1	lysophospholipase 1	Rattus noviegicus	NM_013006	5'-GCTAGAATTACCATGTCGCGCAACACATGTCCGC-3'	5'-GCTAGAATTCGAATTTGGAGTAGGAGCTTAT-3'
Lypla2	lysophospholipase 2	Rattus noviegicus	NM_031342	5'-GCTAGAATTACCATGTGTGTTAAACAATGCTGT-3'	5'-GCTAGAATTCGACCGGAGGCAAGTTTCTCCA-3'
PPT2	palmitoyl protein thioesterase 2	Rattus noviegicus	NM_019367	5'-GCTAGAATTACCATGCGGCTGCTGAGGCGAGAG-3'	5'-GCTAGAATTCGGTGGCTGGGAGCTCT-3'
ABHD2	abhydrolase domain containing 2	Mus musculus	NM_018811	5'-GCTAGAATTACCATGAGCGCTGCTGAGGACCC-3'	5'-GCTAAGATCTTCCAACTCGGCTCCATCTGC-3'
ABHD3	abhydrolase domain containing 3	Mus musculus	NM_134130	5'-GCTAGAATTACCATGAGCGCTGGCCATGAGCT-3'	5'-GCTAGAATTCATGTTGGAGATTCATGTCGTGC-3'
ABHD4	abhydrolase domain containing 4	Mus musculus	NM_134076	5'-GCTAGAATTACCATGAGCGCTGAGCTGAGCT-3'	5'-GCTAGGTACCATGAGTGGAGTCTCTTCTA-3'
ABHD5	abhydrolase domain containing 5	Mus musculus	NM_026179	5'-GCTAGGTACCATGAGGAGGATGGCGCGGAGG-3'	5'-GCTAGGTACCATGAGTGGAGATCTCTT-3'
ABHD6	abhydrolase domain containing 6	Mus musculus	NM_025341	5'-GCTAGAATTACCATGAGTCTGAGCTGAGCT-3'	5'-GCTAAGATCTGTCAGCTTCTTGTGTTGTTAT-3'
ABHD7	abhydrolase domain containing 7	Mus musculus	NM_001001804	5'-GCTAGGTACCATGAGCGCGCGCGCGCGCC-3'	5'-GCTAGGTACCATCTCTCTCTTCTTCTTCTCAGGA-3'
ABHD8	abhydrolase domain containing 8	Mus musculus	NM_022419	5'-GCTAGAATTACCATGAGCTCAGAACACACCATGCTG-3'	5'-GCTAGAATTCCTTCTCTCTCTGAGCGCGG-3'
ABHD10	abhydrolase domain containing 10	Mus musculus	NM_172511	5'-GCTAGAATTACCATGCGGCTGCGGCGCTTGT-3'	5'-GCTAAGATCTACAGCTTTCACACTGTAGTTCGG-3'
ABHD11	abhydrolase domain containing 11	Mus musculus	NM_145215	5'-GCTAGAATTACCATGCTGCTGGCGCGAGCG-3'	5'-GCTAAGATCTAGCAAGAGCTGGTGACAGCATC-3'
ABHD12	abhydrolase domain containing 12	Mus musculus	NM_024465	5'-GCTAAGATCTACCATGAGGAGCGGAGCGAGCCCGT-3'	5'-GCTAAGATCTGCTGGCGTTCGGGTTCCGACT-3'
ABHD13	abhydrolase domain containing 13	Mus musculus	NM_001081119	5'-GCTATTAAATTAACCATGGAATCTCTGGATGCTGTGGA-3'	5'-GCTAGGTACCATGATGATGATGATGATGATGTTT-3'
ABHD16A	abhydrolase domain containing 16A	Mus musculus	NM_178592	5'-GCTAGAATTACCATGCGGAGGCTCTGAGCTGCGCT-3'	5'-GCTAGGTACCATGAGTGGAGGCAATCTGGAAGT-3'
ABHD17B	abhydrolase domain containing 17B	Mus musculus	NM_146096	5'-GCTAAGATCTCAACTGCAAGATGAATATCTGT-3'	5'-GCTAAGATCTCAAAATTTTACCAGTCTCTGTGAACG-3'
ABHD17C	abhydrolase domain containing 17C	Mus musculus	NM_133722	5'-GCTAGAATTACCATGCGGCGCGCGCGCGAGGAT-3'	5'-GCTAAGATCTGAGTGGAGGCTCGTGAGATAT-3'
Dpp8	dipeptidylpeptidase 8	Mus musculus	NM_028906	5'-GCTAGGTACCATGAAATACCATCAGGAAGTGAAC-3'	5'-GCTAGGTACCATCTTTCAGAGCAGCGATACGC-3'
Lipe	hormon sensitive lipase	Mus musculus	NM_010719.5	5'-GCTATTAAATTAACCATGAGCGCGCTGGAATCGG-3'	5'-GCTAGGTACCATCTCAGTGGTGGAGCGGCGG-3'
Fasn-TE	fatty acid synthase (thioesterase domain)	Mus musculus	NM_007988	5'-GCTAGGTACCATGATGACACGTCTTGAAGCAGAAC-3'	5'-GCTAGGTACCATCTCCCTCCCTACACTCCTC-3'
Aadac1 (NCEH1)	neutral cholesterol ester hydrolasee 1	Mus musculus	NM_178772	5'-GCTAGAATTACCATGAGTGCCTGCTCTACTG-3'	5'-GCTAAGATCTCAGGTTTGTATCCAGCCATTGATGT-3'
Faah	fatty acid amide hydrolase	Mus musculus	NM_010173	5'-GCTAGAATTACCATGCTGAGCGAAGTCTGTGC-3'	5'-GCTAGGTACCATGAGTGGCGCTTTTCAGGGGTCA-3'
Lypla1	lysophospholipase 1	Mus musculus	NM_008866	5'-GCTAGAATTACCATGCGGCAACACATGTCGCG-3'	5'-GCTAAGATCTAATCAATGGAGGTAGGAGCTTAT-3'
Lypla2	lysophospholipase 2	Mus musculus	NM_011942	5'-GCTAGAATTACCATGCTGTAACACCATGCTGTGC-3'	5'-GCTAAGATCTGACCGGAGGCAAGTTCCTCCA-3'
Lypla1	lysophospholipase like 1	Mus musculus	NM_146106	5'-GCTAGAATTACCATGGCTGCTGTGCCAGCGCTG-3'	5'-GCTAAGATCTTCACTCTGCCCATCTGTCTCTCC-3'
Plaah2	platelet-activating factor acetylhydrolase 2	Mus musculus	NM_133880	5'-GCTAGAATTCAAAATCCCGAGCACCCGCTTTG-3'	5'-GCTAGAATTCATAGATAGACAGATAGTGGGGGC-3'
PGAP1	post-GPI attachment to proteins 1	Mus musculus	NM_001163314	5'-GCTAGTTAAATTAACCATGTTCTCCTCAGTCAACCTCT-3'	5'-GCTAGGTACCATAAAGTTGCATAACCATGGAACA-3'
PNPLA8	patatin like domain containing 8	Mus musculus	NM_026164	5'-GCTAAGATCTACCATGCTCTAATTTGATCTAGATATAT-3'	5'-GCTAAGATCTCAATTTTGAAGAAATGGAAGGCGCTTC-3'
PPT1	palmitoyl protein thioesterase 1	Mus musculus	NM_008917	5'-GCTAGAATTACCATGCGCTGCTCTGTTCCGGAG-3'	5'-GCTAAGATCTCTTAAGAAAGATGATGTGGCGAG-3'

Table 2 miRNA target sequences and top/bottom oligo DNAs

Target gene	Target position	Target sequence	Top oligo DNA	Bottom oligo DNA
ABHD1	630-651	5'-CTCTTTCGGAGGGATACTGG-3'	5'-TGCTGACCAAGTATCCCTCCGAAGAGGTTTTGGCCACTGACTGACCTCTTTGGGGATACTGGT-3'	5'-CCTGACCAAGTATCCCGAAGAGGTCAGTCAAGTGGCCAAAACCTCTTTGGGAGGATACTGGTC-3'
ABHD3	443-464	5'-TCACTGGAACAAGCAAGGAA-3'	5'-TGCTGATTCCTTGCTGTTCACAGTAGTTTTGGCCACTGACTGACTCACTGGAAGCAAGGAAT-3'	5'-CCTGATTCCTTGCTTTCCAGTAGTCAAGTCAAGTGGCCAAAACCTCACTGGAACAAGCAAGGAATC-3'
ABHD4	163-184	5'-AAGTTCCTGGCCCGTTATGT-3'	5'-TGCTGTACATAACGGGCCAGGAACCTGTTTTGGCCCACTGACTGACAAGTTCTCTCCCGTTATGTA-3'	5'-CCTGTACATAACGGGAGGAACCTTGTCAGTCAGTGGCCAAAACAAGTTCTCTGGCCCGTTATGTAC-3'
ABHD12	291-312	5'-ACAGGCCAAACTGATATCT-3'	5'-TGCTGAAGAATATCAGTTTTGGCCTGTGTTTTGGCCCACTGACTGACACAGGCCACTGATATCTT-3'	5'-CCTGAAGAATATCAGTGGCCTGTGTCAGTCAGTGGCCAAAACACAGGCCCAAACTGATATTTCTTC-3'
ABHD13	286-307	5'-GCGCCTGAATCTGATCTTGG-3'	5'-TGCTGACCAAGATCAGATTACAGCGCGGTTTTGGCCCACTGACTGACGCGCCCTGACTGATCTTGGT-3'	5'-CCTGACCAGATCAGTCAGGCGCGTCAGTCAGTGGCCAAAACGCGCCTGAAATCTGATCTTGGTC-3'
ABHD16A	674-695	5'-CTCCGTGTACTGCTGCTCCAGA-3'	5'-TGCTGTTCTGGAGCAGGTACACGGAGGTTTTGGCCCACTGACTGACCTCCGTTCTGCTCCAGAA-3'	5'-CCTGTTCTGGAGCAGACACGGAGGTCAGTCAGTGGCCAAAACCTCCGTGACTGCTCCAGAAC-3'
ABHD17A	474-495	5'-TGAGAAAGAACCTCTATGCTG-3'	5'-TGCTGTACAGCATAGAGGTCTTCTCAGTTTTGGCCCACTGACTGACTGAGAAGACTCTATGCTGA-3'	5'-CCTGTACAGCATAGAGTCTTCTCAGTCAGTCAGTGGCCAAAACCTGAGAAGAAACCTCTATGCTGAC-3'
ABHD17B	611-632	5'-ATACCAAGAGAACCTTACTGT-3'	5'-TGCTGAACAGTAGGTCTTCTTGATGTTTTGGCCCACTGACTGACATACCAAGGACCTTACTGTT-3'	5'-CCTGAACAGTAGGTCTTGGTATGTCAGTCAGTGGCCAAAACATACCAAGAGACCTTACTGTTTC-3'
ABHD17C	443-464	5'-CGCGCATCACTGCAACATC-3'	5'-TGCTGAGATGTTGCAAGTTGATGCGCGGTTTTGGCCCACTGACTGACCCGGGCATCCTGCAACATCT-3'	5'-CCTGAGATGTTGCAAGATCGCGGGTCAGTCAGTGGCCAAAACCGCGGCATCAACTGCAACATCTC-3'
Lys1a1	199-220	5'-ATGATGATGCGCTTCTTGGTT-3'	5'-TGCTGAACCAAGAGGCATCATGTTTTGGCCCACTGACTGACATGATGATCTTCTTGGTTT-3'	5'-CCTGAACCAAGAGATCATCATGTCAGTCAGTGGCCAAAACATGATGATGCGCTTCTTGGTTTC-3'
Lys1a2	186-207	5'-TCCTGTGACACTCAACATGA-3'	5'-TGCTGTTTCATGTTGAGTGTACAGGAGTTTTGGCCCACTGACTGACTCCTGTGACTCAACATGAA-3'	5'-CCTGTTTCATGTTGAGTGTACAGGAGTCAGTCAGTGGCCAAAACCTCCTGTGACACTCAACATGAAC-3'

Table 3 List of primer pairs for real-time PCR

Target gene	Target region	Forward primer	Reverse primer
GAPDH	729-801	5'-GACATGCCGCCTGGAGAAAC-3'	5'-AGCCCAGGATGCCCTTTAGT-3'
ABHD1	277-351	5'-CAGCCTGTGATCCCTTACCG-3'	5'-CTCAGCCCAGTCCAGAAGGA-3'
	525-606	5'-GCTGACGCACAGGGCTTACT-3'	5'-TCGGGAGTAGCGGTGCTTTA-3'
ABHD2	623-756	5'-TGGGTGGTAACATCGTGTGC-3'	5'-ACACTGGTCCCCTGTCATGA-3'
	1010-1119	5'-TCATGCTGGTCAATGCTGCT-3'	5'-ATGCAGAGGCAGCACAAACA-3'
ABHD3	123-223	5'-CGTCGCCTATGCCTGCTACT-3'	5'-GTCCTGTAGGAAGCGGCTGA-3'
	616-754	5'-CACAGCCTGTACCCTTTGGC-3'	5'-AAGTGTTCAGCCAACCGAA-3'
ABHD4	132-239	5'-GGAAGCCAGGATCCTCCAGT-3'	5'-TCCTTTTGCTCTGGGCTCAC-3'
	921-1014	5'-CACCAGCACAGGGAAGG-3'	5'-GTCAGCGTAGACATGGTGCG-3'
ABHD12	278-402	5'-GTCCTGGGATACAGGCCAAA-3'	5'-ATCCTCGGGCTGGAGGTAGT-3'
	896-977	5'-GGTTCTTCTCGACCCCAATT-3'	5'-AGCAGGGGACAGGAGATGTG-3'
ABHD13	152-248	5'-TGTCGATTGCAGGCATCTTG-3'	5'-CCCGTAGGCATGGGAACATA-3'
	468-574	5'-TGAAGGGGAAGCCAGTGAAG-3'	5'-GGCCGAAAAGGAAAACCTTG-3'
ABHD16A	599-696	5'-TCAAGAAGCTGCCCTGTCAA-3'	5'-GGCCTTCTGGAGCAGGTACA-3'
	968-1066	5'-TCCCACAGAATGAGGCCAAT-3'	5'-TGGACCAGGCGTAGATGACA-3'
ABHD16B	235-367	5'-CAGTGCCTCCTCCAGCAGAT-3'	5'-CGCGCGTCATCAAGAACATA-3'
	574-686	5'-GCACCTCTGGAGGCTGGATA-3'	5'-TTGACCACCACATCCATTGC-3'
ABHD17A	531-630	5'-CATCATCCACGGCACAGAAG-3'	5'-CAGGACCACTGCAGCACACT-3'
	744-893	5'-CATCATCCACGGCACAGAAG-3'	5'-CGTAGGCGCTCCAGGTATTG-3'
ABHD17B	79-116	5'-GCATTCTTGCCACCTGATCC-3'	5'-AGTCCGCTCGTTCTGACAGG-3'
	515-597	5'-GGACCGTACCGTCTGTGGAC-3'	5'-CCGCATTCTGAGGTCAAAG-3'
ABHD17C	607-704	5'-ATTGGCACTGTCCCCACTGT-3'	5'-GGAAAAGCAACACGCAATCC-3'
	728-850	5'-TTGATGCTTTCCCCAGCATT-3'	5'-GGGGACAGCGCTCATACATC-3'
Lypla1	76-170	5'-TTCCTTCACGATTGGGAGA-3'	5'-GGCGCATGTGGACAGATGTA-3'
	358-446	5'-CAGGGAGGCGCCTTATCTTT-3'	5'-CGAAGTGAAGCCAGCAACT-3'
Lypla2	139-246	5'-ATCCGGCTTCTCATGTCAA-3'	5'-ACTCAGCCCCATCAGGTCAA-3'
	281-364	5'-AGGCCGCAGAGAACATCAAG-3'	5'-AAAAGCCACCCAGGACGATT-3'

Table 4 Calculated molecular weights of PEGylated proteins

Protein	gel (%)	mPEG	Molecular weight (kDa)			
			Original	Mono (1-0)	Di (2-1)	Tri (3-2)
PSD-95	6	5k	97.5	106.4 (8.9)	118.6 (12.2)	-
Calnexin	6	5k	101.1	116.1 (15.0)	132.2 (16.5)	-
Hras	14	2k	25.4	28.9 (3.5)	31.1 (2.2)	-
Nras	14	2k	24.7	27.4 (2.7)	-	-
G α_s	10	2k	55.0	57.9 (2.9)	-	-
G α_q	10	2k	45.5	48.0 (2.5)	51.3 (3.3)	-
Cav1	14	2k	23.8	27.4 (3.6)	31.3 (3.9)	35.4 (4.1)

*Molecular weights were calculated by the standard curve of mobility of marker proteins.

Table 5 α/β hydrolase fold regions of mouse ABHD and Lypla proteins used to construct the phylogenetic tree

Protein	α/β hydrolase fold		amino acid number of domain
	start	end	
Lypla1	12	225	213
Lypla2	25	227	202
Lypla1	12	229	217
ABHD1	107	396	289
ABHD2	106	406	300
ABHD3	117	402	285
ABHD4	71	351	280
ABHD5	67	347	280
ABHD6	51	326	275
ABHD7	68	351	283
ABHD8	149	409	260
ABHD9	131	418	287
ABHD10	44	289	245
ABHD11	49	306	257
ABHD12	140	395	255
ABHD13	87	319	232
ABHD14A	45	246	201
ABHD14B	4	209	205
ABHD15	117	410	293
ABHD16A	252	479	227
ABHD16B	139	382	243
ABHD17A	84	305	221
ABHD17B	65	286	221
ABHD17C	97	317	220

Table 6 Contrasting characteristics of the APEGS assay and previous methods for S-palmitoylation analysis

	Chemical exchange		Metabolic labeling	
	APEGS	ABE	[³ H]-palmitate labeling	Click chemistry
Determine the number of sites	○	×	×	×
Determine the stoichiometry	○	×	×	×
Sample	Cultured cells Tissues Purified proteins	Cultured cells Tissues Purified proteins	Cultured live cells	Cultured live cells
Time required	A few days	A few days	Week - month	A few days
Recovery of proteins	High	Low	Depend on IP	Low
Proteomics	×	○	×	○

* APEGS, Acyl-PEGyl exchange; ABE, Acyl-Biotinyl exchange; IP, immunoprecipitation.

References

- Bellizzi, J. J., Widom, J., Kemp, C., Lu, J. Y., Das, A. K., Hofmann, S. L., and Clardy, J., *Proc. Natl. Acad. Sci. USA.*, **97**, 4573-4578 (2000) The crystal structure of palmitoyl protein thioesterase 1 and the molecular basis of infantile neuronal ceroid lipofuscinosis.
- Bernazzani, L., Borsacchi, S., Catalano, D., Gianni, P., Mollica, V., Vitelli, M., Asaro, F., and Feruglio, L., *J. Phys. Chem. B*, **108**, 8960-8969 (2004) On the interaction of sodium dodecyl sulfate with oligomers of poly (ethylene glycol) in aqueous solution.
- Blanchetot, C., Chagnon, M., Dube, N., Halle, M., and Tremblay, M. L., *Methods*, **35**, 44-53 (2005) Substrate-trapping techniques in the identification of cellular PTP targets.
- Brown, D. A., *Physiology*, **21**, 430-439 (2006) Lipid rafts, detergent-resistant membranes, and raft targeting signals.
- Bruger, M., Zimmermann, T. J., Kondoh, Y., Stege, P., Watanabe, N., Osada, H., Waldmann, H., and Vetter, I. R., *J. Lipid Res.*, **53**, 43-50 (2012) Crystal structure of the predicted phospholipase LYPLAL1 reveals unexpected functional plasticity despite close relationship to acyl protein thioesterases.
- Burgoyne, J. R., Oviolu, O., and Eaton, P., *J. Pharmacol. Toxicol. Methods*, **68**, 297-301 (2013) The PEG-switch assay: A fast semi-quantitative method to determine protein reversible cysteine oxidation.
- Camp, L. A., and Hofmann, S. L., *J. Biol. Chem.*, **268**, 22566-22574 (1993) Purification and properties of a palmitoyl-protein thioesterase that cleaves palmitate from H-Ras.

- Cantu, D. C., Chen, Y., and Reilly, P. J., *Protein Sci.*, **19**, 1281-1295 (2010) Thioesterases: a new perspective based on their primary and tertiary structures.
- Charron, G., Zhang, M. M., Yount, J. S., Wilson, J., Raghavan, A. S., Shamir, E., and Hang, H. C., *J. Am. Chem. Soc.*, **131**, 4967-4975 (2009) Robust fluorescent detection of protein fatty-acylation with chemical reporters.
- Chen, L., Chetkovich, D. M., Petralia, R. S., Sweeney, N. T., Kawasaki, Y., Wenthold, R. J., Brecht, D. S., and Nicoll, R. A., *Nature*, **408**, 936-943 (2000) Stargazin regulates synaptic targeting of AMPA receptors by two distinct mechanisms.
- Child, M. A., Hall, C. I., Beck, J. R., Ofori, L. O., Albrow, V. E., Garland, M., Bowyer, P. W., Bradley, P. J., Powers, J. C., Boothroyd, J. C., Weerapana, E., and Bogoy, M., *Nat. Chem. Biol.*, **9**, 651-656 (2013) Small-molecule inhibition of a depalmitoylase enhances *Toxoplasma* host-cell invasion.
- Cho, K. O., Hunt, C. A., and Kennedy, M. B., *Neuron*, **9**, 929-942 (1992) The rat brain postsynaptic density fraction contains a homolog of the *Drosophila* discs-large tumor suppressor protein.
- Couvertier, S. M., Zhou, Y., and Weerapana, E., *Biochim. Biophys. Acta*, **1844**, 2315-2330 (2014) Chemical-proteomic strategies to investigate cysteine posttranslational modifications.
- Craven, S. E., El-Husseini, A. E., and Brecht, D. S., *Neuron*, **22**, 497-509 (1999) Synaptic targeting of the postsynaptic density protein PSD-95 mediated by lipid and protein

motifs.

- Cygler, M., Grochulski, P., Kazlauskas, R. J., Schrag, J. D., Bouthillier, F., Rubin, B., Serreqi, A. N., and Gupta, A. K., *J. Am. Chem. Soc.*, **116**, 3180-3186 (1994) A structural basis for chiral preferences of lipases.
- Davda, D., El Azzouny, M. A., Tom, C. T. M. B., Hernandez, J. L., Majmudar, J. D., Kennedy, R. T., and Martin, B. R., *ACS Chem. Biol.*, **8**, 1912-1917 (2013) Profiling targets of the irreversible palmitoylation inhibitor 2-bromopalmitate.
- Dekker, F. J., Rocks, O., Vartak, N., Menninger, S., Hedberg, C., Balamurugan, R., Wetzel, S., Renner, S., Gerauer, M., Scholermann, B., Rusch, M., Kramer, J. W., Rauh, D., Coates, G. W., Brunsfeld, L., Bastiaens, P. I., and Waldmann, H., *Nat. Chem. Biol.*, **6**, 449-456 (2010) Small-molecule inhibition of APT1 affects Ras localization and signaling.
- Dennis, E. A., Cao, J., Hsu, Y. H., Magrioti, V., and Kokotos, G., *Chem. Rev.*, **111**, 6130-6185 (2011) Phospholipase A2 enzymes: physical structure, biological function, disease implication, chemical inhibition, therapeutic intervention.
- Devedjiev, Y., Dauter, Z., Liznetsov, S. R., Jones, T. L., and Derewenda, Z. S., *Structure*, **8**, 1137-1146 (2000) Crystal structure of the human acyl protein thioesterase I from a single X-ray data set to 1.5 Å.
- Dietzen, D. J., Hasings, W. R., and Lublin, D. M., *J. Biol. Chem.*, **270**, 6838-6842 (1995) Caveolin is palmitoylated on multiple cysteine residues. Palmitoylation is not necessary

for localization of caveolin to caveolae.

Drisdell, R. C., and Green, W. N., *Biotechniques*, **36**, 276-285 (2004) Labeling and quantifying sites of protein palmitoylation.

Duncan, J. A., and Gilman, A. G., *J. Biol. Chem.*, **273**, 15830-15837 (1998) A cytoplasmic acyl-protein thioesterase that removes palmitate from G protein α subunits and p21^{RAS}.

El-Husseini, A. E., Schnell, E., Chetkovich, D. M., Nicoll, R. A., and Brecht, D. S., *Science*, **290**, 1364-1368 (2000a) PSD-95 involvement in maturation of excitatory synapses.

El-Husseini, A. E., Craven, S. E., Chetkovich, D. M., Firestein, B. L., Schnell, E., Aoki, C., and Brecht, D. S., *J. Cell Biol.*, **148**, 159-172 (2000b) Dual palmitoylation of PSD-95 mediates its vesiculotubular sorting, postsynaptic targeting, and ion channel clustering.

El-Husseini, A. E., Schnell, E., Dakoji, S., Sweeny, N., Zhou, Q., Prange, O., Gauthier-Campbell, C., Aguilera-Moreno, A., Nicoll, R. A., and Brecht, D. S., *Cell*, **108**, 849-863 (2002) Synaptic strength regulated by palmitate cycling on PSD-95.

El-Husseini, A. E., and Brecht, D. S., *Nat. Rev. Neurosci.*, **3**, 791-802 (2002) Protein palmitoylation : a regulator of neuronal development and function.

Elias, G. M., Funke, L., Stein, V., Grant, S. G., Brecht, D. S., and Nicoll, R. A., *Neuron*, **52**, 307-320 (2006) Synapse-specific and developmentally regulated targeting of AMPA receptors by a family of MAGUK scaffolding proteins.

Fukata, M., Fukata, Y., Adesnik, H., Nicoll, R. A., and Brecht, D. S., *Neuron*, **44**, 987-996 (2004) Identification of PSD-95 palmitoylating enzymes.

- Fukata, Y., and Fukata, M., *Nat. Rev. Neurosci.*, **11**, 161-175 (2010) Protein palmitoylation in neuronal development and synaptic plasticity.
- Fukata, Y., Dimitrov, A., Boncompain, G., Vielemeyer, O., Perez, F., and Fukata, M., *J. Cell Biol.*, **202**, 145-161 (2013) Local palmitoylation cycles define activity-regulated postsynaptic subdomains.
- Gonzalo, S., and Linder, M. E., *Mol. Biol. Cell*, **9**, 585-597 (1998) SNAP-25 palmitoylation and plasma membrane targeting require a functional secretory pathway.
- Gouy, M., Guindon, S., and Gascuel, O., *Mol. Biol. Evol.*, **27**, 221-224 (2010) SeaView version 4: a multiplatform graphical user interface for sequence alignment and phylogenetic tree building.
- Greaves, J., Prescott, G. R., Fukata, Y., Fukata, M., Salaun, C., and Chamberlain, L. H., *Mol. Biol. Cell*, **20**, 1845-1854 (2009) The hydrophobic cysteine-rich domain of SNAP25 couples with downstream residues to mediate membrane interactions and recognition by DHHC palmitoyl transferases.
- Grimm, D., Lee, J. S., Wang, L., Desai, T., Akache, B., Storm, T. A., and Kay, M. A., *J. Virol.*, **82**, 5887-5911 (2008) In vitro and in vivo gene therapy vector evolution via multispecies interbreeding and retargeting of adeno-associated viruses.
- Grochulski, P., Bouthillier, F., Kazlauskas, R. J., Serreqi, A. N., Schrag, J. D., Ziomek, E., and Cygler, M., *Biochemistry*, **33**, 3494-3500 (1994) Analogs of reaction intermediates identify a unique substrate binding site in *Candida rugosa* lipase.

- Hancock, J. F., Magee, A. I., Childs, J. E., and Marshall, C. J., *Cell*, **57**, 1167-1177 (1989) All ras proteins are polyisoprenylated but only some are palmitoylated.
- Hannoush, R. N., and Arenas-Ramirez, N., *ACS Chem. Biol.*, **4**, 581-587 (2009) Imaging the lipidome: omega-alkynyl fatty acids for detection and cellular visualization of lipid-modified proteins.
- Howie, J., Reilly, L., Fraser, N. J., Viachaki-Walker, J. M., Wypijewski, K. J., Ashford, M. L., Calaghan, S. C., McClafferty, H., Tian, L., Shipston, M. J., Boguslavskyi, A., Shattock, M. J., and Fuller, W., *Proc. Natl. Acad. Sci. USA*, **111**, 17534-17539 (2014) Substrate recognition by the cell surface palmitoyl transferase DHHC5.
- Kang, R., Wan, J., Arstikatis, P., Takahashi, H., Hung, K., Bailey, A. O., Thompson, J. X., Roth, A. F., Drisdel, R. C., Mastro, R., Green, W. N., Yates, J. R. I., Davis, N. G., and El-Husseini, A. E., *Nature*, **456**, 904-909 (2008) Neural palmitoyl-proteomics reveals dynamic synaptic palmitoylation.
- Kim, E., and Sheng, M., *Nat. Rev. Neurosci.*, **5**, 771-781 (2004) PDZ domain proteins of synapses.
- Kienesberger, P. C., Lass, A., Preiss-Landl, K., Wolinski, H., Kohlwein, S. D., Zimmermann, R., and Zechner, R., *J. Biol. Chem.*, **283**, 5908-5917 (2008) Identification of an insulin-regulated lysophospholipase with homology to neuropathy target esterase.
- Kong, E., Peng, S., Chandra, G., Sarkar, C., Zhang, Z., Bagh, M. B., and Mukherjee, A. B., *J. Biol. Chem.*, **288**, 9112-9125 (2013) Dynamic palmitoylation links cytosol-membrane

shuttling of acyl-protein thioesterase-1 and acyl-protein thioesterase-2 with that of proto-oncogene H-ras product and growth-associated protein-43.

Lakkaraju, A. K., Abrami, L., Lemmin, T., Blaskovic, S., Kunz, B., Kihara, A., Dal Peraro, M., and van der Goot, F. G., *EMBO J.*, **31**, 1823-1835 (2012) Palmitoylated calnexin is a key component of the ribosome-translocon complex.

Larkin, M. A., Blackshields, G., Brown, N. P., Chenna, R., McGettigan, P. A., McWilliam, H., Valentin, F., Wallace, I. M., Wilm, A., Lopez, R., Thompson, J. D., Gibson, T. J., and Higgins, D. G., *Bioinformatics*, **23**, 2947-2948 (2007) Clustal W and Clustal X version 2.0.

Lenfant, N., Hotelier, T., Velluet, E., Bourne, Y., Marchot, P., and Chatonnet, A., *Nucleic Acids Res.*, **41**, D423-429 (2013) ESTHER, the database of the α/β -hydrolase fold superfamily of proteins: tools to explore diversity of functions.

Levental, I., Grzybek, M., and Simons, K., *Biochemistry*, **49**, 6305-6316 (2010) Greasing their way: lipid modifications determine protein association with membrane rafts.

Linder, M. E., Middleton, P., Hepler, J. R., Taussig, R., Gilman, A. G., and Mumby, S. M., *Proc. Natl. Acad. Sci. USA*, **90**, 3675-3679 (1993) Lipid modifications of G proteins: alpha subunits are palmitoylated.

Linder, M. E., and Deschenes, R. J., *Nat. Rev. Mol. Cell Biol.*, **8**, 74-84 (2007) Palmitoylation: policing protein stability and traffic.

Lord, C. C., Thomas, G., and Brown, J. M., *Biochim. Biophys. Acta*, **1831**, 792-802 (2013)

Mammalian alpha beta hydrolase domain (ABHD) proteins: Lipid metabolizing enzymes at the interface of cell signaling and energy metabolism.

Magee, A. I., Koyama, A. H., Malfer, C., Wen, D., and Schlesinger M. J., *Biochim. Biophys. Acta*, **798**, 156-166 (1984) Release of fatty acids from virus glycoproteins by hydroxylamine.

Makmura, L., Hamann, M., Areopagita, A., Furuta, S., Munoz, A., and Momand, J., *Antioxid. Redox Singal.*, **3**, 1105-1118 (2001) Development of a sensitive assay to detect reversibly oxidized protein cysteine sulfhydryl groups.

Martin, B. R., and Cravatt B. F., *Nat. Methods*, **6**, 135-138 (2009) Large-scale profiling of protein palmitoylation in mammalian cells.

Martin, B. R., Wang, C., Adibekian, A., Tully, S. E., and Cravatt, B. F., *Nat. Methods*, **9**, 84-89 (2011) Global profiling of dynamic protein palmitoylation.

Mogensen, J. E., Sehgal, P., and Otzen, D. E., *Biochemistry*, **44**, 1719-1730 (2005) Activation, inhibition, and destabilization of *Thermomyces lanuginosus* lipase by detergents.

Nardini, M., and Dijkstra, B. W., *Curr. Opin. Struc. Biol.*, **9**, 732-737 (1999) α/β hydrolases fold enzymes: the family keeps growing.

Noritake, J., Fukata, Y., Iwanaga, T., Hosomi, N., Tsutsumi, R., Matsuda, N., Tani, H., Iwanari, H., Mochizuki, Y., Kodama, T., Matsuura, Y., Brecht, D. S., Hamakubo, T., and Fukata, M., *J. Cell Biol.*, **186**, 147-160 (2009) Mobile DHHC palmitoylating enzyme mediates activity-sensitive synaptic targeting of PSD-95.

- Parenti, M., Vigano, M. A., Newman, C. M. H., Milligan, G., and Magee, A. I., *Biochem. J.*, **291**, 349-353 (1993) A novel N-terminal motif for palmitoylation of G-protein alpha subunits.
- Reichel, C., *Methods Mol. Biol.*, **869**, 65-79 (2012) SARCOSYL-PAGE: a new electrophoretic method for the separation and immunological detection of PEGylated proteins.
- Resh, M. D., *Biochim. Biophys. Acta*, **1451**, 1-16 (1999) Fatty acylation of proteins: new insights into membrane targeting of myristoylated and palmitoylated proteins.
- Resh, M. D., *Sci. STKE.*, **359**, re14 (2006) Palmitoylation of ligands, receptors, and intracellular signaling molecules.
- Rexach, J. E., Rogers, C. J., Yu, S. H., Tao, J., Sum, Y. E., and Hsieh-Wilson, L. C., *Nat. Chem. Biol.*, **6**, 645-651 (2010) Quantification of O-glycosylation stoichiometry and dynamics using resolvable mass tags.
- Roth, A. F., Wan, J., Bailey, A. O., Sun, B., Kuchar, J. A., Green, W. N., Phinney, B. S., Yates, J. R., and Davis, N. G., *Cell*, **125**, 1003-1013 (2006) Global analysis of protein palmitoylation in yeast.
- Roy, S., Plowman, S., Rotblat, B., Prior, I. A., Muncke, C., Grainger, S., Parton, R. G., Henis, Y. I., Kloog, Y., and Hancock, J. F., *Mol. Cell. Biol.* **25**, 6722-6733 (2005) Individual palmitoyl residues serve distinct roles in H-ras trafficking microlocalization, and signaling.

- Schlesinger, M. J., Magee, A. I., and Schmidt, M. F., *J. Biol. Chem.*, **255**, 10021-10024 (1980) Fatty acid acylation of proteins in cultured cells.
- Schmidt, M. F., Bracha, M., and Schlesinger, M. J., *Proc. Natl. Acad. Sci. USA*, **76**, 1687-1691 (1979) Evidence for covalent attachment of fatty acids to Sindbis virus glycoproteins.
- Sefton, B. M., Trowbridge, I. S., and Cooper, J. A., *Cell*, **31**, 465-474 (1982) The transforming proteins of Rous sarcoma virus, Harvey sarcoma virus and Abelson virus contain tightly bound lipid.
- Soding, J., Biegert, A., and Lupas, A. N., *Nucleic Acids Res.*, **33**, W244-248 (2005) The HHpred interactive server for protein homology detection and structure prediction.
- Staufenbiel, M., *Mol. Cell. Biol.*, **7**, 2981-2984 (1987) Ankyrin-bound fatty acid turns over rapidly at the erythrocyte plasma membrane.
- Staufenbiel, M., *J. Biol. Chem.*, **263**, 13615-13622 (1988) Fatty acids covalently bound to erythrocyte proteins undergo a differential turnover *in vitro*.
- Tian, L., McClafferty, H., Knaus, H. G., Ruth, P., and Shipston, M. J., *J. Biol. Chem.*, **287**, 14718-14725 (2012) Distinct acyl protein transferases and thioesterases control surface expression of calcium-activated potassium channels.
- Tomatis, V. M., Trench, A., Gomez, G. A., and Daniotti, J. L., *PLoS One*, **5**, e15045 (2010) Acyl-protein thioesterase 2 catalyses the deacylation of peripheral membrane-associated GAP-43.

- Topinka, J. R., and Bredt, D. S., *Neuron*, **20**, 125-134 (1998) N-terminal palmitoylation of PSD-95 regulates association with cell membranes and interaction with K⁺ channel Kv1.4.
- Tsutsumi, R., Fukata, Y., Noritake, J., Iwanaga, T., Perez, F., and Fukata, M., *Mol. Cell. Biol.*, **29**, 435-447 (2009) Identification of G protein α subunit-palmitoylating enzymes.
- Veger, R., *Trends Biotechnol.*, **15**, 32-38 (1997) Interfacial activation of lipases: facts and artifacts.
- Wan, J., Roth, A. F., Bailey, A. O., and Davis, N. G., *Nat. Protoc.*, **2**, 1573-1584 (2007) Palmitoylated proteins: purification and identification.
- Wedegaertner, P. B., Chu, D. H., Wilson, P. T., Levis, M. J., and Bourne, H. R., *J. Biol. Chem.*, **268**, 25001-25008 (1993) Palmitoylation is required for signaling functions and membrane attachment of Gq α and Gs α .
- Webb, Y., Hermida-Matsumoto, L., and Resh, M. D., *J. Biol. Chem.*, **275**, 261-270 (2000) Inhibition of protein palmitoylation, raft localization, and T cell signaling by 2-bromopalmitate and polyunsaturated fatty acids.
- Wessel, D., and Flugge, U. I., *Anal. Biochem.*, **138**, 141-143 (1984) A method for the quantitative recovery of protein in dilute solution in the presence of detergents and lipids.
- Yagi, H., Ogura, T., Mizukami, H., Urabe, M., Hamada, H., Yoshikawa, H., Ozawa, K., and Kume, A., *J. Gene. Med.*, **13**, 114-122 (2011) Complete restoration of phenylalanine oxidation in phenylketonuria mouse by a self-complementary adeno-associated virus

vector.

Yang, W., Di Vizio, D., Kirchner, M., Steen, H., and Freeman, M. R., *Mol. Cell. Proteomics*, **9**, 54-70 (2010) Proteome scale characterization of human S-acylated proteins in lipid raft-enriched and non-raft membranes.

Zhang, F. L., and Casey, P. J., *Annu. Rev. Biochem.*, **65**, 241-269 (1996) Protein prenylation : molecular mechanisms and functional consequences.

Zhang, M. M., Tsou, L. K., Charron, G., Raghavan, A. S., and Hang, H. C., *Proc. Natl. Acad. Sci. USA*, **107**, 8627-8632 (2010) Tandem fluorescence imaging of dynamic S-acylation and protein turnover.